Quantum algorithm for an additive approximation of Ising partition functions

Akira Matsuo,[1] Keisuke Fujii,[2,3] and Nobuyuki Imoto[1]

[1]*Graduate School of Engineering Science, Osaka University, Toyonaka, Osaka, 560-8531, Japan*

[2]*The Hakubi Center for Advanced Research, Kyoto University, Yoshida-Ushinomiya-cho, Sakyo-ku, Kyoto 606-8302, Japan*

[3]*Graduate School of Informatics, Kyoto University, Yoshida Honmachi, Sakyo-ku, Kyoto 606-8501, Japan*

(Received 13 May 2014; published 5 August 2014)

We investigate quantum-computational complexity of calculating partition functions of Ising models. We construct a quantum algorithm for an additive approximation of Ising partition functions on square lattices. To this end, we utilize the overlap mapping developed by M. Van den Nest, W. Dür, and H. J. Briegel [Phys. Rev. Lett. **98**, 117207 (2007)] and its interpretation through measurement-based quantum computation (MBQC). We specify an algorithmic domain, on which the proposed algorithm works, and an approximation scale, which determines the accuracy of the approximation. We show that the proposed algorithm performs a nontrivial task, which would be intractable on any classical computer, by showing that the problem that is solvable by the proposed quantum algorithm is BQP-complete. In the construction of the BQP-complete problem coupling strengths and magnetic fields take complex values. However, the Ising models that are of central interest in statistical physics and computer science consist of real coupling strengths and magnetic fields. Thus we extend the algorithmic domain of the proposed algorithm to such a real physical parameter region and calculate the approximation scale explicitly. We found that the overlap mapping and its MBQC interpretation improve the approximation scale exponentially compared to a straightforward constant-depth quantum algorithm. On the other hand, the proposed quantum algorithm also provides partial evidence that there exist no efficient classical algorithm for a multiplicative approximation of the Ising partition functions even on the square lattice. This result supports the observation that the proposed quantum algorithm also performs a nontrivial task in the physical parameter region.

DOI: 10.1103/PhysRevA.90.022304 PACS number(s): 03.67.Ac, 03.67.Lx, 75.10.Hk

I. INTRODUCTION

Classical spin models have been widely studied in statistical physics for a long time as simplified pictures of magnetic materials. The Ising model is the simplest model consisting of two-state discrete spin variables, up and down, but exhibits a rich enough structure to be applied to not only magnetic materials but also lattice gases [1], binary alloys, neural systems [2], and economic models [3]. One of the main goals is to calculate a partition function, which tells us statistical properties of a system in thermodynamic equilibrium, such as free energy, magnetization, specific heat, and so on. Many techniques have been developed to calculate the Ising partition functions in both exact and approximated manners. Only the restricted type of Ising models, such as Ising models on two-dimensional planar lattices without magnetic fields, are exactly solvable [4,5]. In general, exact calculation of Ising partition functions belongs to #P-hard problems, which are highly intractable in classical computing [6]. Furthermore, even an efficient (multiplicative) approximation of antiferromagnetic Ising partition functions on general lattices does not exist unless RP = NP [7,8], which is highly implausible [9,10]. It is a natural question how a quantum computer is useful in this context [11,12].

Recently, quantum information theory shed new light on the computational complexity of Ising partition functions. Bravyi and Raussendorf argued the classical simulatability of measurement-based quantum computation (MBQC) [13] on a planar surface code by mapping it into an Ising partition function on a planar lattice [14]. Van den Nest *et al.* established a correspondence between the quantum-stabilizer formalism and classical spin models [15]. In this mapping, a partition function of a classical spin model is expressed as an overlap between a stabilizer state and a product state. This overlap mapping allows us to apply powerful results obtained in the context of quantum information theory to statistical physics [15,16]. Although a transfer matrix approach and a state overlap have already appeared in an earlier work [12], the overlap mapping makes the problem much more tractable, allowing us to interpret the overlap as MBQC and associated quantum circuits. For example, Van den Nest *et al.* showed that the Ising model on a square lattice is complete in the sense that a partition function of any classical spin model on an arbitrary graph can be expressed as a certain instance of it [17,18]. De las Cuevas *et al.* have shown that all classical spin models can be unified as a four-dimensional lattice gauge theory with real coupling constants [19,20]. Such a unification has been achieved not only for the discrete spin variables but also for the statistical models with continuous variables [21]. Furthermore, by using the overlap mapping, classical simulatability of MBQC on certain stabilizer states provides an efficient classical algorithm to calculate the corresponding partition functions [15,22].

Based on the overlap mapping, De las Cuevas *et al.* have proposed a quantum algorithm to approximate partition functions of classical spin models, such as Ising, Potts, vertex, and gauge models, in a complex parameter regime [23]. Furthermore, they showed that additive approximations of certain classical spin models are BQP-complete. (BQP stands for bounded-error quantum polynomial time computation and is a class of decision problems that can be efficiently solved by a quantum computer.) This means that all problems that are solvable by a quantum computer can be mapped into these problems. The consequences of this result are twofold.

First, at least for these types of classical spin models, we can utilize a quantum computer to estimate their partition functions efficiently. Second, BQP-completeness implies that there is less of a possibility to do this task using a classical one. (If it were possible, we could simulate a quantum computer by a classical computer, which is highly implausible.)

In addition, the quantum-computational complexity of not only Ising partition functions but also link invariants such as Jones and Tutte polynomials has also been argued in the circuit models [24–28], and their additive approximations have been shown to be BQP-complete. Recently, a sampling problem related to Ising partition functions was shown to be classically intractable, although it can be done by using commutable quantum circuits [29], so-called instantaneous quantum polynomial time computation (IQP), which seems to be much weaker than universal quantum computation [30]. These results provide a clue to understanding not only the complexity of calculating classical spin partition functions but also problems that are solvable by a quantum computer and the origin of a quantum speedup.

In this paper, we further investigate the complexity of calculating Ising partition functions based on the overlap mapping [15] and its interpretation through MBQC. We specifically consider a quantum algorithm that approximates Ising partition functions on square lattices, where each instance of the problem is encoded into the coupling strengths and magnetic fields. In this sense, the present work is complimentary to the work done in Refs. [23,31], where instances of the problem are encoded into the topology of the graphs while keeping the coupling strengths and magnetic fields constant. Furthermore, we specify a domain, in which the proposed quantum algorithm works, and an approximation scale, which determines the accuracy of the additive approximation. We also provide proof that the problem solved by the proposed quantum algorithm is BQP-hard. This indicates that the proposed quantum algorithm performs a nontrivial task, which would be intractable on any classical computer.

We also establish a way to approximate general Ising partition functions including real coupling strengths and magnetic fields, which are especially of interest in statistical physics. The proposed quantum algorithm for the general Ising partition functions on a square lattice allows us to approximate partition functions of any classical spin model by virtue of the universality result [17]. In a general parameter region, however, the gate operations performed by MBQC are no longer unitary and are linear operators in general. Thus we construct a quantum algorithm that approximates such a linear operator following the method used in Refs. [24,26]. This allows us to calculate the approximation scale for general coupling strengths and magnetic fields.

We should note that related work has recently been done by Iblisdir *et al.* [28]. In their work, certain types of quantum circuits are mapped into the Ising partition functions on square lattices. Specifically, they utilize a transfer matrix approach to map quantum circuits into the Ising partition functions. (A similar approach was also taken in an earlier work [12].) The construction of the quantum algorithm in this work can be regarded as a measurement-based version of these earlier studies, which would be simpler for people who are familiar with MBQC. In Ref. [28], the authors have also considered the approximation of the Ising partition functions with real coupling strengths and magnetic fields, although a rather different approach, analytic continuation, was taken (see also a related work [11]). Instead of analytic continuation, here we straightforwardly simulate linear operators by using unitary circuits. Since the proposed quantum algorithm provides the approximation scale explicitly for all parameter regions, the proposed quantum algorithm allows us to compare the performances. Furthermore, the quantum circuits that approximate the physical Ising partition functions can also be written down explicitly, which would be helpful for understanding the performance of the proposed quantum algorithm in the physical parameter region.

Unfortunately, it is still unknown whether or not the proposed quantum algorithm performs a nontrivial task in the physical parameter region. However, we also provide partial evidence that a multiplicative approximation of the Ising partition functions in the physical parameter region cannot be attained by any classical computer unless the polynomial hierarchy collapses at the third level. This result strongly supports the fact that the proposed quantum algorithm actually performs a nontrivial task even in the physical parameter region. We believe these quantum algorithms in the real parameter regime and their approximation scales provide an essential clue to understanding the potential of quantum computation in solving combinatorial optimization problems.

The rest of this paper is organized as follows. In Sec. II, we review the correspondence between the quantum stabilizer formalism and the Ising partition functions by defining the notation. In Sec. III, we propose a quantum algorithm that approximates the Ising partition functions on square lattices. We also show that the proposed quantum algorithm solves a BQP-complete problem and hence performs a nontrivial task, which would be intractable on any classical computer. In Sec. IV, we extend the domain of the proposed quantum algorithm to general coupling strengths and magnetic fields, which include real parameters. We calculate the approximation scale of the quantum algorithm in this domain and demonstrate the performance of the proposed quantum algorithm in the physical parameter region. Section V is devoted to conclusions and discussion.

II. QUANTUM FORMULATION OF THE ISING MODEL

In this section, we briefly review the correspondence between the quantum-stabilizer formalism and Ising partition functions by defining the notation. We consider a classical Ising model defined on a graph $G = (V,E)$, with V and E being sets of vertices and edges, respectively. The Ising model consists of classical two-state spin variables $\sigma_a = \pm 1$ defined on each vertex $a \in V$ of graph G. Two spins, σ_a and σ_b, connected by an edge $\{a,b\} \in E$ interact with each other by a coupling strength J_{ab}. Furthermore, each spin σ_a is subjected to a local magnetic field h_a. The Hamiltonian of the system is given by

$$H_G(\boldsymbol{\sigma}) = -\sum_{\{a,b\}\in E} J_{ab}\sigma_a\sigma_b - \sum_{a\in V} h_a\sigma_a, \tag{1}$$

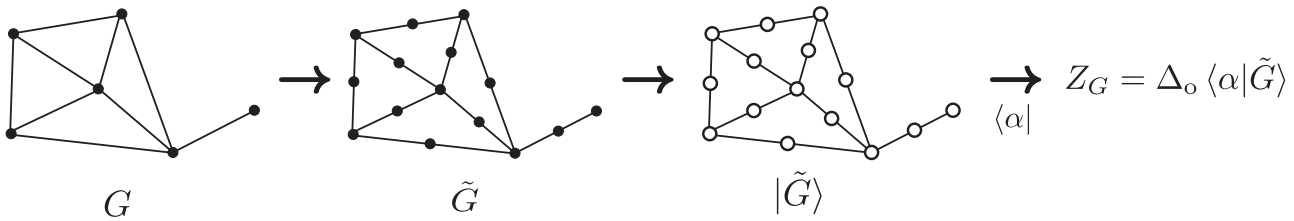

FIG. 1. Graph G, the corresponding decorated graph $\tilde{G}$, and the decorated graph state $|\tilde{G}\rangle$ (from the left to the right). The partition function of the Ising model on a graph G is related to an inner product between the graph state $|\tilde{G}\rangle$ and a product state $|\alpha\rangle$ defined in Eqs. (6)–(8) with an approximation scale Δ_o.

where $\boldsymbol{\sigma}$ indicates a spin configuration. The partition function is defined by

$$Z_G = \sum_{\boldsymbol{\sigma}} e^{-\beta H_G(\boldsymbol{\sigma})}, \tag{2}$$

where the summation $\sum_{\boldsymbol{\sigma}}$ is taken over all spin configurations and β is the inverse temperature, $\beta = 1/k_B T$, with k_B and T being the Boltzmann constant and the temperature, respectively.

We express the partition function as an inner product between a product state and a stabilizer state [17]. We first define the stabilizer state, which is described as a graph state associated with another graph $\tilde{G}$. Graph $\tilde{G} = (\tilde{V}, \tilde{E})$, which we call a decorated graph, is defined by adding a vertex on each edge of graph G, as shown in Fig. 1. The decorated graph $\tilde{G}$ has $|\tilde{V}| = |V| + |E|$ vertices and $|\tilde{E}| = 2|E|$ edges. The set of vertices $\tilde{V}$ is defined by $\tilde{V} = V \cup V_E$, where $V_E = \{e_{ab} | \{a,b\} \in E\}$ corresponds to the set of vertices added on the edges. The set of edges $\tilde{E}$ is defined by $\tilde{E} = \{\{a, e_{ab}\} | a,b \in V, e_{ab} \in V_E\}$. Assigning a qubit on each vertex in $\tilde{V}$, we define a $|\tilde{V}|$-qubit stabilizer state:

$$|\varphi_{\tilde{G}}\rangle = 2^{-|V|/2} \sum_{\boldsymbol{s}} \bigotimes_{e_{ab} \in V_E} |s_a \oplus s_b\rangle \bigotimes_{a \in V} |s_a\rangle, \tag{3}$$

where $s_a = 0,1$, $\sum_{\boldsymbol{s}}$ is taken over all configurations of $\boldsymbol{s} \equiv \{s_a\}$, and $s_a \oplus s_b$ indicates the addition modulo 2. The binary variable $s_a = 0,1$ is related to the Ising spin $\sigma_a = \pm 1$ below. The qubits belonging to V and V_E are referred to as vertex and edge qubits, respectively. We can easily confirm $|\varphi_{\tilde{G}}\rangle$ is a stabilizer state since it can be obtained as

$$|\varphi_{\tilde{G}}\rangle = \left[\prod_{a \in V} \prod_{e \in \tilde{\mathcal{N}}_a} \Lambda_{a,e}(X) \right] \bigotimes_{a \in V} |+\rangle \bigotimes_{e \in V_E} |0\rangle, \tag{4}$$

where $\Lambda_{i,j}(A)$ indicates the controlled-A gate between qubits i (control) and j (target) and $\tilde{\mathcal{N}}_a \subseteq V_E$ denotes the set of vertices adjacent to vertex $a \in V$ on the decorated graph $\tilde{G}$. Let $|\tilde{G}\rangle$ be the graph state associated with graph $\tilde{G}$ [32]. Using the equality $\Lambda_{i,j}(X) = H_j \Lambda_{i,j}(Z) H_j$, $|\varphi_{\tilde{G}}\rangle$ is related to the graph state $|\tilde{G}\rangle$ as follows:

$$\begin{aligned} |\varphi_{\tilde{G}}\rangle &= \left(\prod_{e_{ab} \in V_E} H_{e_{ab}} \right) \left[\prod_{a \in V} \prod_{e \in \tilde{\mathcal{N}}_a} \Lambda_{a,e}(Z) \right] |+\rangle^{\otimes |V| + |V_E|} \\ &= \left(\prod_{e_{ab} \in V_E} H_{e_{ab}} \right) |\tilde{G}\rangle, \end{aligned} \tag{5}$$

where $H_{e_{ab}}$ is the Hadamard gate acting on edge qubit e_{ab}.

Next, we define a product state by which the stabilizer state $|\varphi_{\tilde{G}}\rangle$ is taken as an inner product:

$$|\alpha\rangle = \bigotimes_{e_{ab} \in V_E} H |\alpha_{e_{ab}}\rangle \bigotimes_{a \in V} |\alpha_a\rangle, \tag{6}$$

where the single-qubit states are defined as

$$\langle \alpha_{e_{ab}}| = \frac{e^{\beta J_{ab}} \langle 0|_{e_{ab}} + e^{-\beta J_{ab}} \langle 1|_{e_{ab}}}{\sqrt{|e^{\beta J_{ab}}|^2 + |e^{-\beta J_{ab}}|^2}}, \tag{7}$$

$$\langle \alpha_a| = \frac{e^{\beta h_a} \langle 0|_a + e^{-\beta h_a} \langle 1|_a}{\sqrt{|e^{\beta h_a}|^2 + |e^{-\beta h_a}|^2}} \tag{8}$$

for all vertices $e_{ab} \in V_E$ and $a \in V$.

Now, we relate the Ising partition function to the inner product between the product state $|\alpha\rangle$ and the graph state $|\tilde{G}\rangle$ as follows:

$$Z_G = \Delta_o \left(\bigotimes_{e_{ab} \in V_E} \langle \alpha_{e_{ab}}| \bigotimes_{a \in V} \langle \alpha_a| \right) |\varphi_{\tilde{G}}\rangle = \Delta_o \langle \alpha | \tilde{G} \rangle, \tag{9}$$

where the approximation scale Δ_o is defined by

$$\begin{aligned} \Delta_o = 2^{|V|/2} &\prod_{\{a,b\} \in E} \sqrt{|e^{\beta J_{ab}}|^2 + |e^{-\beta J_{ab}}|^2} \\ &\times \prod_{a \in V} \sqrt{|e^{\beta h_a}|^2 + |e^{-\beta h_a}|^2}. \end{aligned} \tag{10}$$

Equation (9) can be understood as follows. The stabilizer state $|\varphi_{\tilde{G}}\rangle$ (or the graph state $|\tilde{G}\rangle$) has information about the geometry of the Ising interactions. More precisely, each vertex qubit has a superposition of spin-up and -down states, and each edge qubit encodes the information about whether the two spins interacting with each other are parallel or antiparallel. Depending on the state of the vertex and edge qubits, weights $e^{\pm \beta h_a}$ and $e^{\pm \beta J_{ab}}$ are assigned by the product state through the inner product. Then, the superposition of all spin states is reduced to the summation over all spin configurations, which recovers the partition functions Z_G on the left-hand side (lhs) of Eq. (9).

Next, we translate the overlap equation (9) into quantum computation, which is one of the most important tasks to establish a bridge between quantum computation and Ising partition functions. States $\langle \alpha_{e_{ab}}|$ and $\langle \alpha_a|$ can be expressed by using unitary gates $A_{e_{ab}}$ and A_a acting on the computational basis state, respectively,

$$\langle \alpha_{e_{ab}}| = \langle 0 | A_{e_{ab}}, \quad \langle \alpha_a| = \langle 0 | A_a, \tag{11}$$

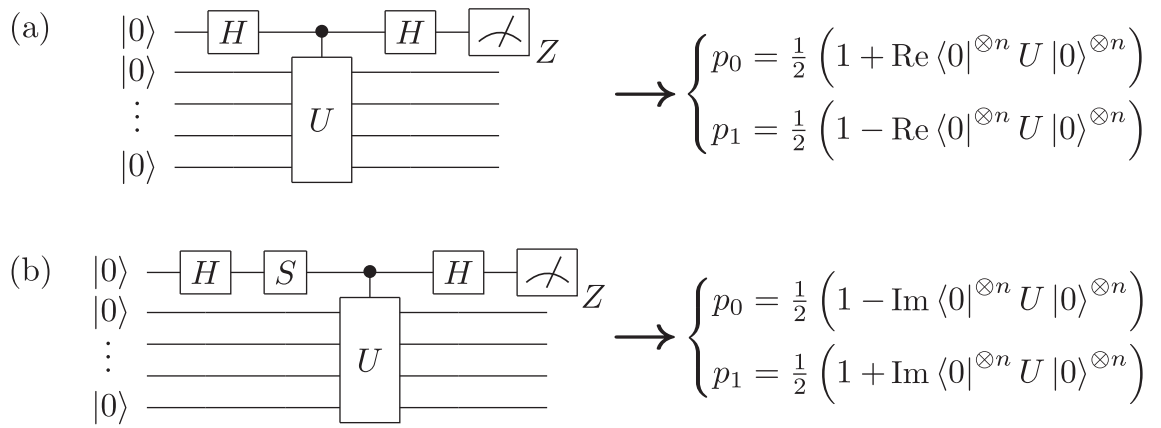

FIG. 2. The Hadamard test to estimate a matrix element $\langle 0|^{\otimes n} U |0\rangle^{\otimes n}$ with an additive error $1/\mathrm{poly}(n)$. The real and imaginary parts of the matrix element, $\mathrm{Re}(\langle 0|^{\otimes n} U |0\rangle^{\otimes n})$ and $\mathrm{Im}(\langle 0|^{\otimes n} U |0\rangle^{\otimes n})$, respectively, are estimated from the probability distributions of the Z-basis measurements in the circuits in (a) and (b), respectively. Here $\mathrm{Re}(\cdot)$ and $\mathrm{Im}(\cdot)$ indicate the real and imaginary parts, respectively.

where we define single-qubit unitary gates

$$A_{e_{ab}} = \frac{1}{\sqrt{|e^{\beta J_{ab}}|^2 + |e^{-\beta J_{ab}}|^2}} \begin{pmatrix} e^{\beta J_{ab}} & e^{-\beta J_{ab}} \\ (e^{-\beta J_{ab}})^* & -(e^{\beta J_{ab}})^* \end{pmatrix}, \quad (12)$$

$$A_a = \frac{1}{\sqrt{|e^{\beta h_a}|^2 + |e^{-\beta h_a}|^2}} \begin{pmatrix} e^{\beta h_a} & e^{-\beta h_a} \\ (e^{-\beta h_a})^* & -(e^{\beta h_a})^* \end{pmatrix}. \quad (13)$$

Then, the product state $\langle \alpha|$ can be rewritten as

$$\langle \alpha| = \langle 0|^{\otimes |V|+|E|} \left(\bigotimes_{e_{ab}\in V_E} A_{e_{ab}} H \right) \left(\bigotimes_{a\in V} A_a \right) \equiv \langle 0|^{\otimes |\tilde{V}|} A, \quad (14)$$

where A is defined as the tensor product of the single-qubit gates. On the other hand, by virtue of the properties of the graph state [33], there exists a $|\tilde{V}|$-qubit unitary gate F such that

$$|\tilde{G}\rangle = F|0\rangle^{\otimes |\tilde{V}|}. \quad (15)$$

Specifically, if the degree of graph $\tilde{G}$ is finite, as considered here, F is a constant-depth Clifford circuit consisting of Hadamard gates and controlled-Z gates. Then, Eq. (9) is rewritten as

$$Z_G = \Delta_{\mathrm{o}} \langle 0|^{\otimes |\tilde{V}|} AF |0\rangle^{\otimes |\tilde{V}|}. \quad (16)$$

The quantum circuit AF consisting of only $\mathrm{poly}(|\tilde{V}|)$ quantum gates can be efficiently implemented on a quantum computer. The matrix element of AF can be estimated using the Hadamard test (see, e.g., [24–26]), as shown in Fig. 2. More precisely, we can obtain an approximation c of $\langle 0|^{\otimes |\tilde{V}|} AF |0\rangle^{\otimes |\tilde{V}|}$ within the following additive error:

$$|c - \langle 0|^{\otimes |\tilde{V}|} AF |0\rangle^{\otimes |\tilde{V}|}| \leqslant \frac{1}{\mathrm{poly}(|\tilde{V}|)}. \quad (17)$$

Accordingly, the partition function Z_G can efficiently be approximated with an additive error $\Delta_{\mathrm{o}}/\mathrm{poly}(|\tilde{V}|)$.

The approximation scale Δ_{o} of the above quantum algorithm is far from optimal since we utilized only constant depth quantum circuits. By using the idea of MBQC, we can compress the number of qubits employed utilizing non-constant-depth quantum circuits. This allows us to improve the approximation scale as follows. The overlap $\langle \alpha|\tilde{G}\rangle$ is regarded as an MBQC implemented by the sequence of projections $\langle \alpha|$ on the resource state $|\tilde{G}\rangle$. If the projection $\langle \alpha|$ satisfies a certain condition such that the MBQC interpretation works appropriately, we can rewrite the overlap as teleportation-based n-qubit quantum computation,

$$\langle \alpha|\tilde{G}\rangle = 2^{-(|\tilde{V}|-n)/2} \langle 0|^{\otimes n} U |0\rangle^{\otimes n}, \quad (18)$$

where U is a non-constant-depth quantum circuit. Note the number n of qubits on the right-hand side (rhs) are reduced compared to $|\tilde{V}|$ on the lhs. By using this identity, Eq. (9) can be rewritten as

$$Z_G = \Delta \langle 0|^{\otimes n} U |0\rangle^{\otimes n}, \quad (19)$$

where an approximation scale is defined as $\Delta \equiv \Delta_{\mathrm{o}} 2^{-(|\tilde{V}|-n)/2}$. By using the Hadamard test to evaluate the rhs, the partition function Z_G is approximated by an additive error $\Delta/\mathrm{poly}(n)$. Note that the approximation scale Δ is exponentially improved from Δ_{o}. On the other hand, computation time is increased only polynomially. Thus we can still obtain an exponential improvement of the accuracy of the approximation taking into account the computation time. The improved approximation scale and the algorithmic domain can be calculated according to the details of how to embed the Ising models in MBQC as done below.

III. A QUANTUM ALGORITHM FOR ISING PARTITION FUNCTIONS

In this section, we propose a quantum algorithm to approximate the partition function of the Ising model by establishing a mapping between a class of Ising models and MBQC.

We consider an Ising model on an $n \times m$ square lattice $G^{n\times m}$ with $m = \mathrm{poly}(n)$ [see Fig. 3(a)]. We define vertical and horizontal coupling strengths, J^{v}_{ab} and J^{h}_{ab}, for the vertical and horizontal edges $\{a,b\}$, respectively. The Hamiltonian is

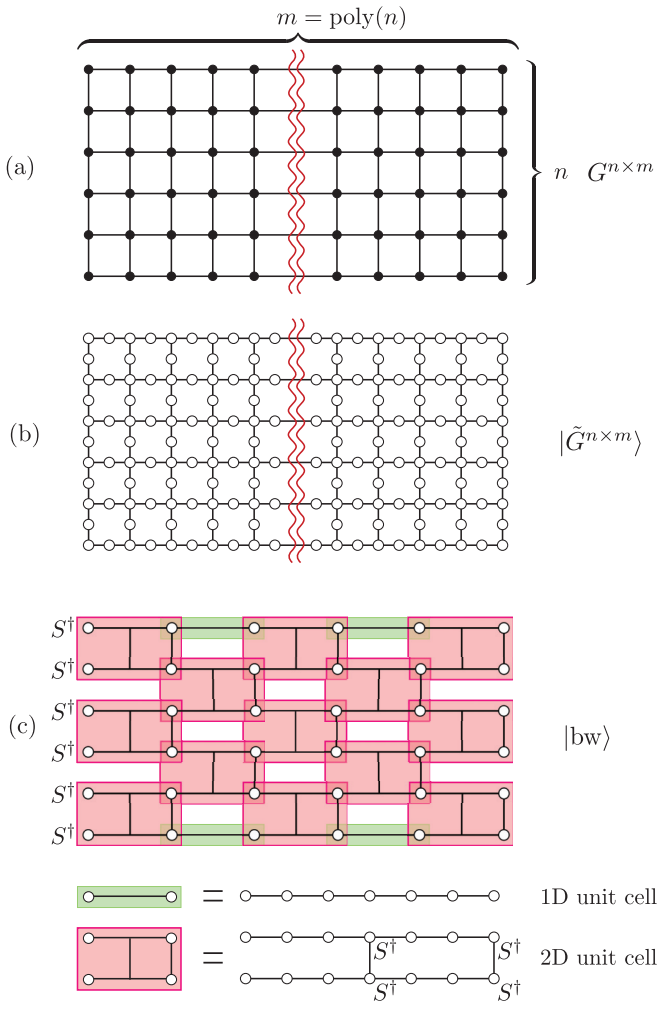

FIG. 3. (Color online) (a) The graph $G^{n\times m}$ on which the Ising model is defined. (b) The corresponding decorated graph state $|\tilde{G}^{n\times m}\rangle$. (c) The brickwork state $|\mathrm{bw}\rangle$ consisting of two-dimensional (2D) unit cells and one-dimensional (1D) unit cells at the top and bottom boundaries.

given by

$$H_{G^{n\times m}}(\boldsymbol{\sigma}) = -\sum_{\{a,b\}\in E^{\mathrm{v}}} J^{\mathrm{v}}_{ab}\sigma_a\sigma_b - \sum_{\{a,b\}\in E^{\mathrm{h}}} J^{\mathrm{h}}_{ab}\sigma_a\sigma_b - \sum_{a\in V} h_a\sigma_a, \tag{20}$$

where E^{v} and E^{h} are the sets of vertical and horizontal edges, respectively. Specifically, we consider the following problem:

Problem 1 (approximation of Ising partition functions). Consider an Ising model on an $n\times m$ square lattice, where $m = \mathrm{poly}(n)$. The magnetic fields $\{\beta h_a\}$ and the vertical coupling strengths $\{\beta J^{\mathrm{v}}_{ab}\}$ are arbitrary imaginary numbers, and the horizontal coupling strengths $\{\beta J^{\mathrm{h}}_{ab}\}$ are given by $\{r_{ab} + i(2k_{ab}+1)\pi/4\}$, where r_{ab} is a real number and k_{ab} is an integer. The problem is defined as an approximation of the partition function $Z_{G^{n\times m}}$ of the given Ising Hamiltonian $H_{G^{n\times m}}$ with an additive error $\Delta/\mathrm{poly}(n)$, where the approximation scale Δ is given by $\Delta = 2^{n(m+1)/2}\prod_{\{a,b\}\in E^{\mathrm{h}}}\sqrt{\cosh(2r_{ab})}$.

In the following sections, we will show two theorems:

Theorem 1 (quantum algorithm). There exists an efficient quantum algorithm that solves Problem 1.

Theorem 2 (BQP-hardness). Problem 1 is BQP-hard.

By combining these results, we will conclude the following theorem:

Theorem 3 (BQP-completeness). Consider Problem 1 and note that $|Z_{G^{n\times m}}|$ is promised to be either $\leqslant\Delta/3$ or $\geqslant 2\Delta/3$. Then the problem to decide whether or not $|Z_{G^{n\times m}}| \leqslant \Delta/3$ is BQP-complete.

A. Construction of a quantum algorithm (proof of Theorem 1)

In this section, we prove Theorem 1. We first construct a quantum algorithm which solves Problem 1. To this end, we interpret horizontal edges of graph $G^{n\times m}$ as wires of an n-qubit quantum circuit. According to the coupling strengths and magnetic fields, quantum gates are assigned on the wires from the left to the right as follows [see Fig. 4(a)]:

(i) $H^{\otimes n}$ are assigned as initial gates.

(ii) According to the vertical coupling strength $\beta J^{\mathrm{v}}_{ab}$, a two-qubit gate $U_{e_{ab}} \equiv e^{\beta J^{\mathrm{v}}_{ab} Z_i Z_j}$ is assigned on the corresponding ith and jth wires. Since $\beta J^{\mathrm{v}}_{ab}$ is an imaginary number, $U_{e_{ab}}$ is a two-qubit unitary gate. Specifically, if $\beta J^{\mathrm{v}}_{ab} = 0$, an identity gate is assigned.

(iii) According to the magnetic field βh_a, a single-qubit gate $U_a \equiv He^{\beta h_a Z_j}$ is assigned on the corresponding jth wire. Since βh_a is an imaginary number, U_a is a single-qubit unitary gate.

(iv) According to the horizontal coupling strength $\beta J^{\mathrm{h}}_{ab}$, we assign a single-qubit gate $U_{e_{ab}} \equiv e^{i(2k_{ab}+1)\pi/4}He^{i\xi_{ab}Z_j}$ on the corresponding jth wire. Here $\xi_{ab}\in[-\pi/2,\pi/2]$ is an angle that satisfies $\sin\xi_{ab} = (-1)^{k_{ab}+1}e^{-r_{ab}}/\sqrt{2\cosh(2r_{ab})}$. [Recall that $\beta J^{\mathrm{h}}_{ab} = r_{ab} + i(2k_{ab}+1)\pi/4$.]

(v) Repeat steps (ii)–(iv) for each column of the decorated graph $\tilde{G}^{n\times m}$ from left to right.

After the above procedure, we obtain a quantum circuit

$$\mathcal{C} = \left(\prod_{\eta\in\tilde{V}^{n\times m}}^{\rightarrow} U_\eta\right) H^{\otimes n}, \tag{21}$$

where the multiplication $\prod^{\rightarrow}_{\eta\in\tilde{V}^{n\times m}}$ is performed over all vertices $\eta\in\tilde{V}^{n\times m}$ of the decorated graph $\tilde{G}^{n\times m}$ from the left to right columns. In the same column, the multiplications for vertical edge qubits are taken first, and those for vertex qubits are taken second.

Next, we will show that the quantum circuit $\mathcal{C}$ is related to the partition function as

$$Z_{G^{n\times m}} \propto \langle\alpha|\tilde{G}^{n\times m}\rangle \propto \langle 0|^{\otimes n}\mathcal{C}|0\rangle^{\otimes n}. \tag{22}$$

We interpret the projection by $\langle\alpha|$ as a sequence of measurements in MBQC, whose resource state is given by the graph state $|\tilde{G}^{n\times m}\rangle$. The measurements are assumed to be performed from left to right. (In the projection $\langle\alpha|$, the measurement outcomes are always determined, and there is no feed-forward in the present MBQC interpretation. Thus we chose a convenient measurement order, from left to right, without loss of generality.) As shown below, the projection by $\langle\alpha|$ induces a sequence of unitary gates in a measurement-

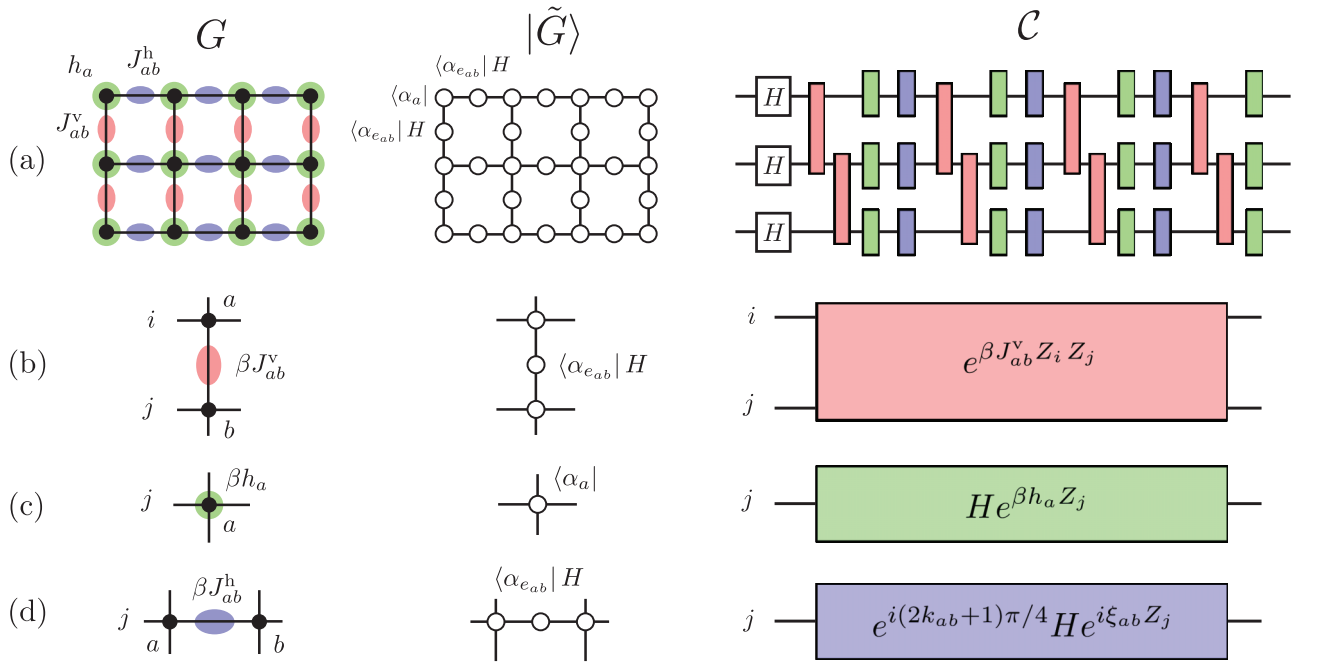

FIG. 4. (Color online) The left column shows the parameters of the Ising model. The middle column shows the projections made on the graph state. The right column shows the resulting quantum gates. (a) The whole picture of constructing the quantum circuits. (b) The vertical coupling strength and the resulting two-qubit gate. (c) The magnetic field and the resulting single-qubit gate. (d) The horizontal coupling strength and the resulting single-qubit gate.

based way, which corresponds to the n-qubit quantum circuit $\mathcal{C}$ constructed.

The projection $\langle\alpha_{e_{ab}}|H = (e^{\beta J^{\rm v}_{ab}}\langle 0| + e^{-\beta J^{\rm v}_{ab}}\langle 1|)H/\sqrt{2}$ on the vertical edge qubit can be written as

$$\langle\alpha_{e_{ab}}|H_{e_{ab}}\Lambda_{a,e_{ab}}(Z)\Lambda_{b,e_{ab}}(Z)|+\rangle_{e_{ab}}|\tilde{G}^{n\times m}\backslash e_{ab}\rangle = \frac{1}{\sqrt{2}}U_{e_{ab}}|\tilde{G}^{n\times m}\backslash e_{ab}\rangle. \tag{23}$$

Here $|\tilde{G}^{n\times m}\backslash e_{ab}\rangle$ indicates a graph state associated with the decorated graph, where vertex e_{ab} and adjacent edges are deleted. This tells us that the projection on the vertical edge qubit on e_{ab} can be replaced by the two-qubit gate $U_{e_{ab}} = e^{\beta J^{\rm v}_{ab} Z_i Z_j}$ on the corresponding wires, as shown in Fig. 4(b).

The projection on the vertex qubit is regarded as quantum teleportation, which propagates quantum information from left to right with a single-qubit unitary gate. The standard argument for MBQC [13] tells us the projection by $\langle\alpha_a| = (e^{\beta h_a}\langle 0| + e^{-\beta h_a}\langle 1|)/\sqrt{2}$ results in the single-qubit gate $U_a = He^{\beta h_a Z_j}$. The projection on the horizontal edge qubit is done with the Hadamard gate:

$$\langle\alpha_{e_{ab}}|H = \left[\cosh\left(\beta J^{\rm h}_{ab}\right)\langle 0| + \sinh\left(\beta J^{\rm h}_{ab}\right)\langle 1|\right]/\sqrt{\cosh(2r_{ab})} = e^{i(2k_{ab}+1)\pi/4}\left(e^{i\xi_{ab}}\langle 0| + e^{-i\xi_{ab}}\langle 1|\right)/\sqrt{2}. \tag{24}$$

Recall that $\xi_{ab} \in [-\pi/2,\pi/2]$ and satisfies $\sin\xi_{ab} = (-1)^{k_{ab}+1}e^{-r_{ab}}/\sqrt{2\cosh(2r_{ab})}$. Similar to the previous case, this projection results in a single-qubit gate $U_{e_{ab}} = e^{i(2k_{ab}+1)\pi/4}He^{i\xi_{ab}Z_j}$.

By repeatedly using the above arguments, we obtain a unitary gate

$$\prod_{a\in V_r} U_a^\dagger \left(\prod_{\eta\in\tilde{V}^{n\times m}}^{\rightarrow} U_\eta\right), \tag{25}$$

where V_r is the set of n vertices of the right boundary of G. The initial state of MBQC is $|+\rangle^{\otimes n} = H^{\otimes n}|0\rangle^{\otimes n}$, and hence the Hadamard gates are implemented on $|0\rangle^{\otimes n}$ as initial gates. The readout of the output qubits is done by the projections $\bigotimes_{a\in V_r}\langle\alpha_a| = \bigotimes_{a\in V_r}(\langle 0|A_a)$ on vertex qubits at the right boundary. Since $A_a = U_a = He^{\beta h_a Z_j}$, $U_a^\dagger$ and A_a are canceled out. This yields the following relation:

$$Z_{G^{n\times m}} = \Delta_{\rm o}\langle\alpha|\tilde{G}^{n\times m}\rangle \propto \langle 0|^{\otimes n}\mathcal{C}|0\rangle^{\otimes n}, \tag{26}$$

where $\Delta_{\rm o} = 2^{|V|+|V_E|/2}\prod_{\{a,b\}\in E^{\rm h}}\sqrt{\cosh(2r_{ab})}$. Since the probability amplitude of the resource state is reduced by $2^{-1/2}$ for each projection in MBQC, we obtain

$$\langle\alpha|\tilde{G}^{n\times m}\rangle = 2^{-(|V|+|V_E|-n)/2}\langle 0|^{\otimes n}\mathcal{C}|0\rangle^{\otimes n}. \tag{27}$$

Thus we conclude that

$$Z_{G^{n\times m}} = \Delta\langle 0|^{\otimes n}\mathcal{C}|0\rangle^{\otimes n}, \tag{28}$$

where we defined the approximation scale

$$\Delta \equiv \Delta_{\rm o}2^{-(|V|+|V_E|-n)/2} = 2^{|V|/2+n/2}\prod_{\{a,b\}\in E^{\rm h}}\sqrt{\cosh(2r_{ab})}. \tag{29}$$

The matrix element $\langle 0|^{\otimes n}\mathcal{C}|0\rangle^{\otimes n}$ can be estimated with an additive error $1/{\rm poly}(n)$ using the Hadamard test (see Fig. 2), which utilizes the controlled-$\mathcal{C}$ gate. Accordingly, the quantum

algorithm consisting of the $(n+1)$-qubit controlled-$\mathcal{C}$ gate and the single-qubit measurement for the Hadamard test approximates the partition function $Z_{G^{n\times m}}$ with an additive error $\Delta/\mathrm{poly}(n)$. While the approximation scale is improved exponentially compared to Δ_{o} for the constant-depth algorithm, it is still unclear whether or not the constructed quantum algorithm performs a nontrivial task, which would be intractable on any classical computer. To provide such evidence, in the next section, we will show Problem 1 is BQP-hard (Theorem 2). That is, we can simulate an arbitrary quantum computation by calculating a partition function with a specific parameter in Problem 1.

B. BQP-hardness (proof of Theorem 2)

In this section, we will prove Theorem 2, that is, BQP-hardness of Problem 1. We define a subproblem of Problem 1:

Problem 2 (BQP-hard subproblem). Consider an Ising model on $G^{n\times m}$ and the corresponding decorated graph state $|\tilde{G}^{n\times m}\rangle$. The magnetic fields are taken homogeneously as $\beta h_a = i\pi/4$. The vertical coupling strengths $\{\beta J^{\mathrm{v}}_{ab}\}$ are chosen to be 0 or $i\pi/4$. The horizontal coupling strengths $\{\beta J^{\mathrm{h}}_{ab}\}$ are chosen to be $i\pi/4$ or $\Omega \equiv \ln(\sqrt{2}+1)/2 + i\pi/4$. Then the problem is defined as an approximation of the partition function $Z_{G^{n\times m}}$ of the given Ising Hamiltonian $H_{G^{n\times m}}$ with an additive error $\Delta/\mathrm{poly}(n)$. The approximation scale is defined as $\Delta = 2^{n(m+1)/2+\#\Omega/4}$, with $\#\Omega$ being the number of horizontal couplings of Ω.

Below, we will show Problem 2 is BQP-hard. We use the fact that the approximation of a matrix element $\langle 0|^{\otimes n} U |0\rangle^{\otimes n}$ of an n-qubit unitary circuit U with an additive error $O(1/\mathrm{poly}(n))$ is BQP-hard [24,34,35]. This is also the case when U consists of a polynomial number of nearest-neighbor two-qubit gates acting on a one-dimensional array of qubits. We have already established the relation between the partition function $Z_{G^{n\times m}}$ and the quantum circuit $\mathcal{C}$ as given in Eq. (28). Thus the goal here is to show that an arbitrary unitary circuit U can be constructed by $\mathcal{C}$ with specific coupling strengths and magnetic fields. This can be shown by using universality of MBQC on certain resource states with a restricted type of projection, which is available in Problem 2. A brickwork state [36,37], a type of graph state, as shown in Fig. 5, is useful for this purpose since we can show universality of MBQC on it with a restricted type of single-qubit measurement. Also, in blind quantum computation, the single-qubit measurements that Alice can command Bob to do in secret are restricted. Thus a brickwork state is utilized to show the capability of universal blind quantum computation using such a restricted type of measurement [37,38].

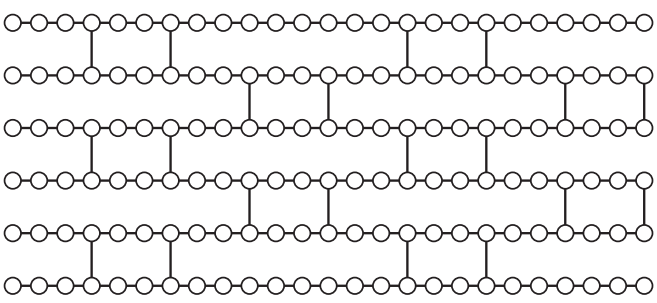

FIG. 5. An example of the brickwork states.

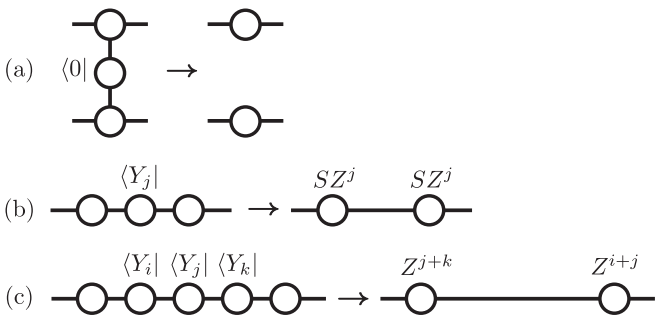

FIG. 6. The rules for transformations of graph states by Pauli-basis projections. (a) Projection $\langle 0|$ on a vertical edge qubit. (b) Projection $\langle Y_j|$ on an edge qubit. State $\langle Y_j|$ $(j=0,1)$ is an eigenstate of the Pauli-Y operator with an eigenvalue $(-1)^j$, i.e., $\langle Y_j| \equiv [\langle 0| - (-1)^j i\langle 1|]/\sqrt{2}$. The local Clifford gate $SZ^j \otimes SZ^j$ is applied as a by-product depending on the projected state $\langle Y_j|$. (c) A sequence of Y projections connects the neighboring qubits directly to the Pauli-Z by-products.

In order to obtain the brickwork state, we transform the graph state using the Pauli-basis projections [33,39]. The transformation rules are summarized in Fig. 6. For example, the Z-basis projection (with eigenvalue $+1$) removes the qubit from the graph state, as shown in Fig. 6(a). The Y-basis projection (with eigenvalue $+1$) connects the adjacent qubits directly to the local Clifford by-product operator $S\otimes S$, as shown in Fig. 6(b), where $S = \mathrm{diag}(1,i)$. Specifically, a sequence of Y-basis projections on three neighboring qubits connects the adjacent qubits directly to the local Z operator, as shown in Fig. 6(c).

We decompose $\langle\alpha|$ into $\langle\alpha| = \langle\gamma| \otimes \langle\delta|$, where the projection $\langle\gamma|$ is used to transform the graph state $|\tilde{G}^{n\times m}\rangle$ into a brickwork state as follows. Let us consider a unit cell $G^{2\times 15}$ of the square lattice $G^{n\times m}$ and the corresponding

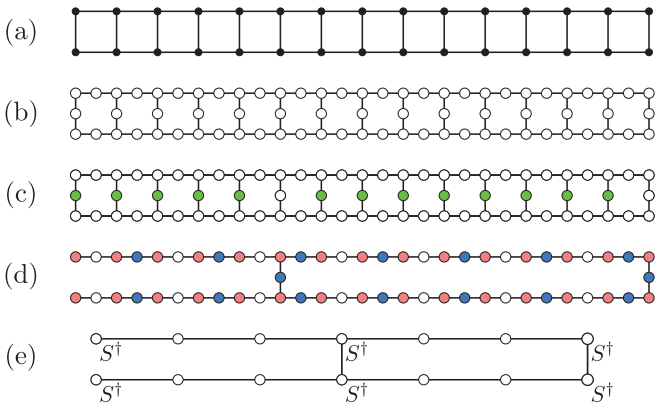

FIG. 7. (Color online) (a) The unit cell $G^{2\times 15}$. (b) The corresponding decorated graph state $|\tilde{G}^{2\times 15}\rangle$. (c) Qubits colored green (light gray) are deleted by the projections $\langle 0|$. (d) Qubits colored by red (medium gray) and blue (dark gray), corresponding to vertex and edge qubits, are projected by $\langle Y_0|$ and $\langle Y_1|$, respectively. (e) After the projections, we obtain the 2D unit cell of the brickwork state up to local Clifford gates shown.

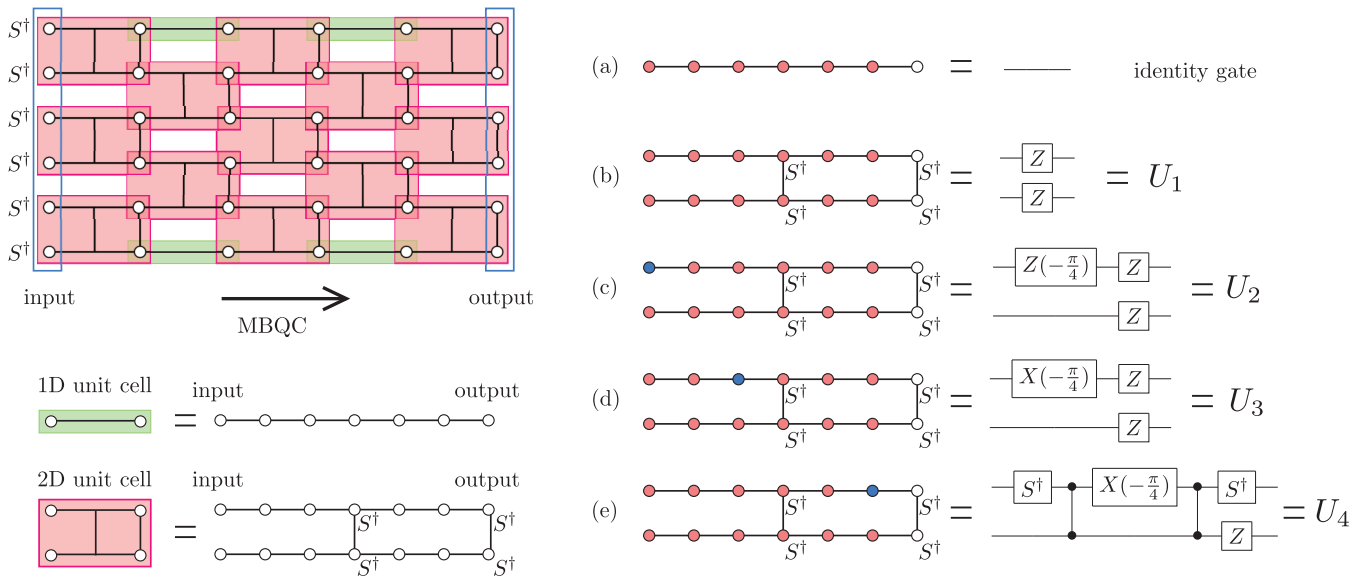

FIG. 8. (Color online) (left) The MBQC interpretation of the projections on the brickwork state. (right) The projections on the 1D and 2D unit cells are translated into one- and two-qubit gates, respectively. The qubits colored red (medium gray) are projected by $\langle Y_1| = \langle +|S = (\langle 0| + i\langle 1|)/\sqrt{2}$, which corresponds to the coupling strength $\beta J^{\rm h}_{ab} = i\pi/4$. The qubits colored blue (dark gray) are projected by $\langle +|T = (\langle 0| + e^{i\pi/4}\langle 1|)/\sqrt{2}$, which corresponds to the coupling strength $\beta J^{\rm h}_{ab} = \Omega$.

decorated graph state $|\tilde{G}\rangle$, as shown in Figs. 7(a) and 7(b), respectively. We perform the Z-basis projections on certain vertical edge qubits, which are colored green (light gray) in Fig. 7(c), to cut the corresponding edges. This is done by choosing the corresponding vertical coupling strengths to be $\beta J^{\rm v}_{ab} = 0$. Next, we perform the Y-basis projections on those qubits colored red (medium gray) and blue (dark gray) in Fig. 7(d). Specifically, the red (medium gray) and blue (dark gray) qubits are projected by $\langle Y_0| \equiv (\langle 0| - i\langle 1|)/\sqrt{2}$ and $\langle Y_1| \equiv (\langle 0| + i\langle 1|)/\sqrt{2}$, respectively. This is done by choosing the corresponding magnetic fields and coupling strengths to be $\beta h_a = i\pi/4$ and $\beta J^{\rm h,v}_{ab} = i\pi/4$, respectively. By using the transformation rules shown in Fig. 6, we obtain a two-dimensional (2D) unit cell of the brickwork state as shown in Fig. 7(e) up to local Clifford gates. If the above projections are made on the square lattice $G^{n\times m}$, the brickwork state with local Clifford gates is prepared as shown in Fig. 3(c), which we define as $|{\rm bw}\rangle$. At the top and bottom boundaries, one-dimensional (1D) unit cells also appear. (We can also consider a square lattice with a periodic boundary condition.)

These projections are described as

$$\langle\alpha|\tilde{G}^{n\times m}\rangle = (\langle\gamma| \otimes \langle\delta|)|\tilde{G}^{n\times m}\rangle = \Delta_{\rm t}\langle\delta|{\rm bw}\rangle, \tag{30}$$

where $\Delta_{\rm t} = 2^{-\#\gamma/2}$, with $\#\gamma$ being the number of the qubits in $\langle\gamma|$, and $\langle\delta|$ is a tensor product of the remaining horizontal edge qubits on the brickwork state.

The brickwork state $|{\rm bw}\rangle$ can be shown to be a universal resource for MBQC using a restricted type of measurement available in Problem 2:

Lemma 1 (universality of the brickwork state). Let U be an arbitrary quantum circuit consisting of a polynomial number of nearest-neighbor two-qubit gates in one dimension. We can always find the horizontal coupling strengths $\beta J^{\rm h}_{ab} \in \{i\pi/4, \Omega\}$ for the unmeasured qubits, such that the projection $\langle\delta|$ on them satisfies

$$\left|\langle 0|^{\otimes n} U |0\rangle^{\otimes n} - \Delta_{\rm c}^{-1}\langle\delta|{\rm bw}\rangle\right| \leqslant \frac{1}{{\rm poly}(n)}, \tag{31}$$

where $\Delta_{\rm c} = 2^{-(\#\delta - n)/2}$, with $\#\delta$ being the number of the qubits in $\langle\delta|$.

Proof of Lemma 1. It is sufficient to show that a universal set of gates can be implemented by choosing the remaining horizontal coupling strengths $\beta J^{\rm h}_{ab}$ from $\{i\pi/4, \Omega\}$. The horizontal coupling strength $\beta J^{\rm h}_{ab} = i\pi/4$ corresponds to the projections by $\langle\alpha_{e_{ab}}|H = \langle +|S$, which results in an HS gate through gate teleportation. Similarly, the horizontal coupling strength $\beta J^{\rm h}_{ab} = \ln(\sqrt{2}+1)/2 + i\pi/4$ corresponds to the projections by $\langle\alpha_{e_{ab}}|H = \langle +|T$, with $T = {\rm diag}(1, e^{i\pi/4})$, which results in a HT gate through gate teleportation. [This can be confirmed by considering special instances of the previous case, as shown in Fig. 4(d).]

As for the 1D unit cell of the brickwork state lying at the boundaries, we can choose the coupling strengths such that the resulting single-qubit gate is an identity gate, as shown in Fig. 8(a). Patterns of the horizontal coupling strengths for the 2D unit cell and the resulting two-qubit gates are shown in Figs. 8(b)–8(e). Specifically, the following two-qubit gates are realized:

$$U_1 = Z \otimes Z, \tag{32}$$

$$U_2 = (Z \otimes Z)\left[Z\left(-\frac{\pi}{4}\right) \otimes I\right], \tag{33}$$

$$U_3 = (Z \otimes Z)\left[X\left(-\frac{\pi}{4}\right) \otimes I\right], \tag{34}$$

$$U_4 = (S^\dagger \otimes Z)\Lambda(Z)\left[X\left(-\frac{\pi}{4}\right) \otimes I\right]\Lambda(Z)(S^\dagger \otimes I), \tag{35}$$

where $X(\theta) \equiv e^{-i\theta X/2}$ and $Z(\theta) \equiv e^{-i\theta Z/2}$. By using these two-qubit gates, the identity gate is constructed as ${U_1}^2$. The single-qubit $\pi/8$ gate is constructed as $T = (U_1U_2)^7$ up to a global phase. $Z(k\pi/4)$ and $X(k\pi/4)$ gates for an integer $k = 0,1,\ldots,7$ are constructed as $Z(k\pi/4) = (U_1U_2)^{8-k}$ and $X(k\pi/4) = (U_1U_3)^{8-k}$, respectively. The Hadamard gate is constructed as $H = Z(\pi/2)X(\pi/2)Z(\pi/2)$. The controlled-NOT gate is constructed as

$$\Lambda_{2,1}(X) = \left[X\left(\frac{\pi}{2}\right)\otimes I\right]\left[Z\left(\frac{\pi}{2}\right)\otimes Z\left(-\frac{\pi}{2}\right)\right]U_4U_1U_4 \times \left[Z\left(\frac{\pi}{2}\right)\otimes I\right]. \tag{36}$$

Since a universal gate set $\{T,H,\Lambda(X)\}$ [35] is constructed, the gate set $\{U_1,U_2,U_3,U_4\}$ is also a universal set of gates. This guarantees that the matrix element $\langle 0|^{\otimes n}U|0\rangle^{\otimes n}$ can be decomposed into a polynomial number of elementary gates $\{U_1,U_2,U_3,U_4\}$ in the sense of an approximation by the Kitaev-Solovay algorithm [35]. This yields

$$\left|\langle 0|^{\otimes n}U|0\rangle^{\otimes n} - \Delta_{\rm c}^{-1}\langle\delta|{\rm bw}\rangle\right| \leqslant \frac{1}{{\rm poly}(n)}, \tag{37}$$

where $\Delta_{\rm c} = 2^{-(\#\delta-n)/2}$, meaning that the probability amplitude is factored by $2^{-1/2}$ at each projection except for the projections for the final readouts of n qubits. ■

By using Lemma 1 and Eqs. (9) and (30), we conclude that

$$|\Delta^{-1}Z_{G^{n\times m}} - \langle 0|^{\otimes n}U|0\rangle^{\otimes n}| \leqslant \frac{1}{{\rm poly}(n)}, \tag{38}$$

with $\Delta = \Delta_{\rm c}\Delta_{\rm t}\Delta_{\rm o} = 2^{|V|/2+\#\Omega/4+n/2}$. This indicates that if we have an approximation $Z^{\rm ap}_{G^{n\times m}}$ of the partition function $Z_{G^{n\times m}}$ with an additive error $\Delta/{\rm poly}(n)$, it satisfies

$$\left|\Delta^{-1}Z^{\rm ap}_{G^{n\times m}} - \langle 0|^{\otimes n}U|0\rangle^{\otimes n}\right| \leqslant \frac{1}{{\rm poly}(n)}. \tag{39}$$

This indicates that Problem 2 is BQP-hard and hence can simulate an arbitrary quantum computation. This completes the proof of Theorem 2.

From Theorems 1 and 2, we conclude that Problem 1 (and also Problem 2), the approximation of the partition functions of the Ising model on a square lattice with an additive error $\Delta/{\rm poly(n)}$, is BQP-complete.

Problem 2 seems to be tight in the sense that some coupling strengths are prohibited; we could not show BQP-hardness. If the horizontal coupling strength Ω is prohibited, the corresponding quantum circuit $\mathcal{C}$ becomes a Clifford circuit and hence is classically simulatable [35]. Similarly, if the vertical coupling strength $i\pi/4$ is prohibited, the corresponding quantum circuit $\mathcal{C}$ is decomposed into single-qubit rotations without any interactions, which apparently is classically simulatable. If the vertical coupling strength $\beta J^{\rm v}_{ab} = 0$ is prohibited, each qubit interacts with nearest-neighbor qubits at every step. Even in such a case, there is a possibility of showing universality by using, for example, the scheme developed by Raussendorf [36], where spatially homogeneous operations with temporal modulations are cleverly employed for universal quantum computation. BQP-hardness in such a case is an open problem for a future work.

Finally, we mention another subproblem of Problem 1, which can also be utilized to show BQP-hardness:

Probelm 3 (another BQP-hard subproblem). The horizontal coupling strengths are chosen to be $\beta J^{\rm h}_{ab} = i\pi/4$. The vertical coupling strengths are chosen to be $\beta J^{\rm h}_{ab} = 0$ or $= i\pi/4$. The magnetic fields βh_a are chosen from $\{0,i\pi/4,i\pi/8\}$. The problem is defined as an approximation of the partition function $Z_{G^{n\times m}}$ of the given Ising Hamiltonian $H_{G^{n\times m}}$ with an additive error $\Delta/{\rm poly}(n)$, where the approximation scale is defined as $\Delta = 2^{n(m+1)/2}$.

Problem 3 is apparently a subproblem of Problem 1. We can also show the BQP-hardness of Problem 3 straightforwardly by following the strategy developed above.

IV. EXTENSION TO GENERAL COUPLING STRENGTHS AND MAGNETIC FIELDS

In the previous section, we formulated the quantum algorithm to approximate the Ising partition functions by using the overlap mapping and its MBQC interpretation, reducing the approximation scale. Unfortunately, the coupling strengths and magnetic fields in Problem 1 take complex values. In this section, we extend the domain of the proposed quantum algorithm to general coupling strengths and magnetic fields, including physical Ising models with real parameters, which are of central interest in statistical physics and computer science. In such a case, the projections are not always mapped into unitary quantum circuits, and nonunitary operations appear. Below we will first explain how to simulate nonunitary operations originating from MBQC in the general parameter region by introducing ancilla qubits. Based on this strategy, the approximation scale Δ for the general domain is calculated. We will confirm that the approximation scale in the previous unitary case can also be obtained as a special case. If coupling strengths and magnetic fields are finite, the approximation scale Δ is always smaller than $\Delta_{\rm o}$ for the constant-depth circuits obtained solely from the overlap mapping.

Unfortunately, we cannot show BQP-hardness inside the physical region with real coupling strengths and magnetic fields. Thus it is still not known if the proposed algorithm performs a nontrivial task inside this domain. However, the extended quantum algorithm also provides partial evidence that there is no efficient multiplicative approximation of the Ising partition functions with the real physical parameters. This result strongly supports the observation that the proposed quantum algorithm performs a nontrivial task even in the physical parameter region.

A. Simulation of linear operators

We first explain how to simulate general liner operators using ancilla qubits and unitary gates, following the scheme developed in Refs. [24,26]. Let M be an arbitrary $d\times d$ matrix acting on a d-dimensional space. The singular value decomposition yields $M = WDP^\dagger$, where W and P are unitary matrices. $D = {\rm diag}(r_1,\ldots,r_d)$ is a diagonal matrix whose diagonal elements are real nonnegative values subject to $r_1 \geqslant r_2 \geqslant \cdots \geqslant r_d \geqslant 0$. The eigenstate with the eigenvalue r_i is denoted $|i\rangle$ for all $i = 1,2,\ldots,d$. If d is finite, it is obvious that W and $P^\dagger$ can be implemented by a quantum

computer. Thus it is sufficient to consider an implementation of the diagonal operator D on a d-dimensional space.

In order to simulate D we utilize an ancilla qubit $|0\rangle$ and a unitary operation $\tilde{D}$ on the composite system,

$$\begin{aligned}\tilde{D} &= \sum_{i=1}^{d} |i\rangle\langle i| \otimes \left[\frac{r_i}{r_1}\Big(|0\rangle\langle 0| + |1\rangle\langle 1|\Big)\right. \\ &\quad \left. + \sqrt{1-\left(\frac{r_i}{r_1}\right)^2}\,(-|0\rangle\langle 1| + |1\rangle\langle 0|)\right] \\ &\equiv \sum_{i=1}^{d} |i\rangle\langle i| \otimes Y(\theta_i), \end{aligned} \tag{40}$$

where $Y(\theta_i) \equiv e^{-i\theta_i Y/2}$ is a Y-rotation gate on the ancilla qubit with an angle $\theta_i \equiv 2\arccos(r_i/r_1) \in [0,\pi]$. Since $Y(\theta_1) = I$, the unitary operator $\tilde{D}$ acts like a controlled-Y-rotation gate, which is controlled by the d-dimensional system. Denoting the input state as $|\psi\rangle|0\rangle = (\sum_{i=1}^{d} c_i|i\rangle)|0\rangle$, this unitary operation yields

$$\tilde{D}\sum_{i=1}^{d} c_i|i\rangle \otimes |0\rangle = \sum_{i=1}^{d} c_i|i\rangle \otimes \left[\frac{r_i}{r_1}|0\rangle + \sqrt{1-\left(\frac{r_i}{r_1}\right)^2}|1\rangle\right]. \tag{41}$$

By projecting the ancilla qubit to $|0\rangle$, we obtain

$$(I \otimes \langle 0|)\tilde{D}\sum_{i=1}^{d} c_i|i\rangle \otimes |0\rangle = \sum_{i=1}^{d} \frac{r_i}{r_1} c_i|i\rangle = \frac{1}{\|M\|} D \sum_{i=1}^{d} c_i|i\rangle, \tag{42}$$

where $\|M\| \equiv r_1$ is an operator one-norm. Thus the linear operator M is simulated as

$$(I \otimes \langle 0|)W\tilde{D}P^{\dagger}(|\psi\rangle \otimes |0\rangle) = \frac{1}{\|M\|} M|\psi\rangle, \tag{43}$$

up to the factor $1/\|M\|$. The simulation of linear operators succeeds only when the ancilla qubit is projected by $\langle 0|$. However, in the proposed quantum algorithm no postselection is required since the matrix element of a unitary circuit including ancilla qubits is estimated by using the Hadamard test, as shown below.

B. Extended quantum algorithm

Now we return to the quantum algorithm for the Ising models with the general parameter regions. The projections in the MBQC interpretation of the overlap Eq. (9) can be classified into two types, types I and II, as depicted in Figs. 9(a) and 9(b), respectively.

Let us first consider a type-I projection with $\langle x| = x_0\langle 0| + x_1\langle 1|$, where x_0 and x_1 are complex numbers with $|x_0|^2 + |x_1|^2 = 1$. For an arbitrary single-qubit input state $|\psi\rangle$, this projection yields

$$(\langle x| \otimes I)\Lambda(Z)(|\psi\rangle \otimes |+\rangle) = \frac{1}{\sqrt{2}} HM|\psi\rangle, \tag{44}$$

where the resultant operator

$$M = \sqrt{2}\,\mathrm{diag}(x_0, x_1) \tag{45}$$

is not a unitary gate in general [see Fig. 9(a)]. The operator one-norm $\|M\|$ is given by $\|M\| = \sqrt{2}\max(|x_0|,|x_1|)$. To simulate this operator M on a quantum computer, we decompose it into $M = DW$, where D is a positive diagonal operator and W is a unitary operator,

$$D = \sqrt{2}\,\mathrm{diag}(|x_0|,|x_1|), \quad W = \mathrm{diag}(e^{i\phi_{x_0}}, e^{i\phi_{x_1}}). \tag{46}$$

Here $\phi_{x_{0,1}} = \arg x_{0,1}$ (i.e., $x_0 = e^{i\phi_{x_0}}|x_0|$ and $x_1 = e^{i\phi_{x_1}}|x_1|$). We introduce an indicator function

$$l = \begin{cases} 0 & \text{if} \quad \left|\frac{x_0}{x_1}\right| \geqslant 1, \\ 1 & \text{if} \quad \left|\frac{x_0}{x_1}\right| < 1. \end{cases} \tag{47}$$

A Y-rotation gate is defined as

$$\begin{aligned} Y(\theta) &= \begin{pmatrix} \cos(\theta/2) & -\sin(\theta/2) \\ \sin(\theta/2) & \cos(\theta/2) \end{pmatrix} \\ &\equiv \begin{pmatrix} \left|\frac{x_1}{x_0}\right|^{(-1)^l} & -\sqrt{1-\left|\frac{x_1}{x_0}\right|^{2(-1)^l}} \\ \sqrt{1-\left|\frac{x_1}{x_0}\right|^{2(-1)^l}} & \left|\frac{x_1}{x_0}\right|^{(-1)^l} \end{pmatrix}, \end{aligned} \tag{48}$$

where the angle $\theta \in [0,\pi]$ is given by

$$\theta = 2\arccos\left(\left|\frac{x_1}{x_0}\right|^{(-1)^l}\right). \tag{49}$$

As previously mentioned, we can simulate M by using the controlled-$Y(\theta)$ gate $\Lambda(Y(\theta))$ as follows:

$$\begin{aligned} \frac{1}{\|M\|} HM|\psi\rangle &= \langle 0|_2 H_1 X_1^l \Lambda_{1,2}(Y(\theta)) X_1^l W_1|\psi\rangle_1|0\rangle_2 \\ &\equiv \langle 0|_2 Q|\psi\rangle_1|0\rangle_2, \end{aligned} \tag{50}$$

where the sequence of the unitary gates is denoted by Q [see the circuit diagram in Fig. 9(a)]. From Eqs. (44) and (50) we obtain

$$\langle x|_1\Lambda_{1,2}(Z)|\psi\rangle_1|+\rangle_2 = \frac{\|M\|}{\sqrt{2}}\langle 0|_2 Q|\psi\rangle_1|0\rangle_2. \tag{51}$$

The type-I projections are made on the vertex qubits and horizontal edge qubits. Specifically, the projection $\langle x|$ on the vertex qubit is described as

$$\langle x| = x_0\langle 0| + x_1\langle 1| = \frac{e^{\beta h_a}\langle 0| + e^{-\beta h_a}\langle 1|}{\sqrt{|e^{\beta h_a}|^2 + |e^{-\beta h_a}|^2}}. \tag{52}$$

The indicator function, angle of the Y rotation, and norm are calculated for each vertex qubit $a \in V$ as

$$l_a = \begin{cases} 0 & \text{if} \quad |e^{2\beta h_a}| \geqslant 1, \\ 1 & \text{if} \quad |e^{2\beta h_a}| < 1, \end{cases} \tag{53}$$

$$\theta_a = 2\arccos(|e^{-(-1)^{l_a}2\beta h_a}|), \tag{54}$$

$$\|M_a\| = \frac{\sqrt{2}|e^{(-1)^{l_a}\beta h_a}|}{\sqrt{|e^{\beta h_a}|^2 + |e^{-\beta h_a}|^2}}. \tag{55}$$

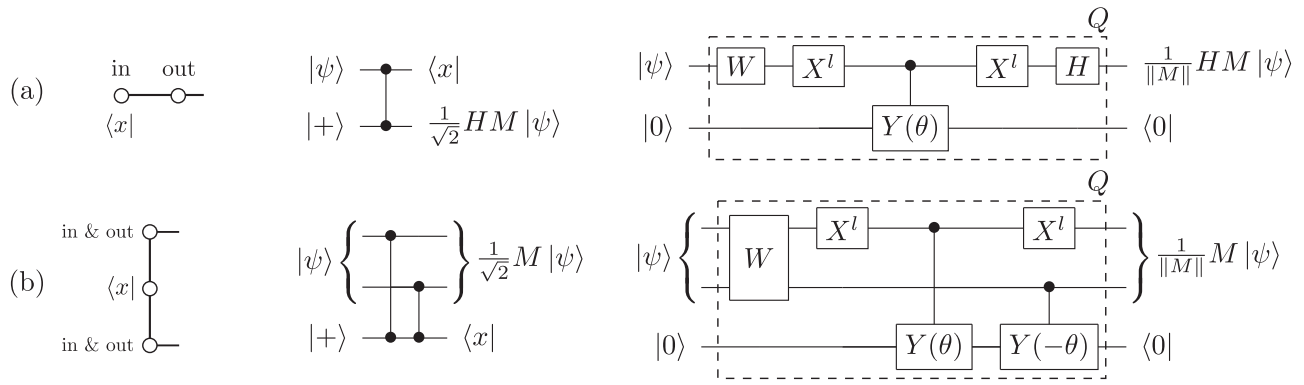

FIG. 9. (left) Projections on the graph states, (middle) the resultant linear operations, and (right) the quantum circuits that simulate the corresponding linear operations. The middle column shows a circuit representation of MBQC of the left column. (a) Projection on vertex and horizontal edge qubits, which we refer to as type-I projection. (b) Projection on a horizontal edge qubit, which we refer to as type-II projection.

In the case of a horizontal edge qubit, the projection is made with the Hadamard gate:

$$\langle x| = x_0\langle 0| + x_1\langle 1| = \frac{e^{\beta J^{\rm h}_{ab}}\langle 0| + e^{-\beta J^{\rm h}_{ab}}\langle 1|}{\sqrt{|e^{\beta J^{\rm h}_{ab}}|^2 + |e^{-\beta J^{\rm h}_{ab}}|^2}}H. \tag{56}$$

Similar to the previous case, the indicator function, angle of the Y rotation, and norm are calculated for each horizontal edge qubit $\{a,b\} \in E^{\rm h}$ as follows:

$$l_{ab} = \begin{cases} 0 & \text{if} \quad \left|\coth\left(\beta J^{\rm h}_{ab}\right)\right| \geqslant 1, \\ 1 & \text{if} \quad \left|\coth\left(\beta J^{\rm h}_{ab}\right)\right| < 1, \end{cases} \tag{57}$$

$$\theta_{ab} = 2\arccos\left[\left|\left\{\tanh\left(\beta J^{\rm h}_{ab}\right)\right\}^{(-1)^{l_{ab}}}\right|\right], \tag{58}$$

$$\|M_{ab}\| = \frac{\left|e^{\beta J^{\rm h}_{ab}} + (-1)^{l_{ab}}e^{-\beta J^{\rm h}_{ab}}\right|}{\sqrt{\left|e^{\beta J^{\rm h}_{ab}}\right|^2 + \left|e^{-\beta J^{\rm h}_{ab}}\right|^2}}. \tag{59}$$

Next, we consider the type-II projection, as shown in Fig. 9(b). A type-II projection with $\langle x| = x_0\langle 0| + x_1\langle 1|$ on an arbitrary two-qubit input state $|\psi\rangle_{1,2}$ yields

$$(I_{1,2} \otimes \langle x|_3)\Lambda_{2,3}(Z)\Lambda_{1,3}(Z)(|\psi\rangle_{1,2} \otimes |+\rangle_3) = \frac{1}{\sqrt{2}}M|\psi\rangle_{1,2}, \tag{60}$$

where M is given by

$$M = \mathrm{diag}(x_0 + x_1, x_0 - x_1, x_0 - x_1, x_0 + x_1) \tag{61}$$

and $\|M\| = \max(|x_0 + x_1|, |x_0 - x_1|)$ [see Fig. 9(b)]. The operator M is decomposed into a positive diagonal operator D and a unitary operator W:

$$D = \mathrm{diag}(|x_0 + x_1|, |x_0 - x_1|, |x_0 - x_1|, |x_0 + x_1|), \tag{62}$$

$$W = \mathrm{diag}(e^{i\phi_{x_0+x_1}}, e^{i\phi_{x_0-x_1}}, e^{i\phi_{x_0-x_1}}, e^{i\phi_{x_0+x_1}}), \tag{63}$$

where $\phi_{x_0\pm x_1} \equiv \arg(x_0 \pm x_1)$ (i.e., $x_0 + x_1 = e^{i\phi_{x_0+x_1}}|x_0 + x_1|$ and $x_0 - x_1 = e^{i\phi_{x_0-x_1}}|x_0 - x_1|$). We introduce an indicator function

$$l = \begin{cases} 0 & \text{if} \quad \left|\frac{x_0+x_1}{x_0-x_1}\right| \geqslant 1, \\ 1 & \text{if} \quad \left|\frac{x_0+x_1}{x_0-x_1}\right| < 1, \end{cases} \tag{64}$$

and a Y-rotation gate

$$Y(\theta) \equiv \begin{pmatrix} \left|\frac{x_0-x_1}{x_0+x_1}\right|^{(-1)^l} & -\sqrt{1 - \left|\frac{x_0-x_1}{x_0+x_1}\right|^{2(-1)^l}} \\ \sqrt{1 - \left|\frac{x_0-x_1}{x_0+x_1}\right|^{2(-1)^l}} & \left|\frac{x_0-x_1}{x_0+x_1}\right|^{(-1)^l} \end{pmatrix}, \tag{65}$$

where the angle $\theta \in [0,\pi]$ is given by

$$\theta = 2\arccos\left(\left|\frac{x_0 - x_1}{x_0 + x_1}\right|^{(-1)^l}\right). \tag{66}$$

Then, the linear operator M is simulated [see the circuit diagram in Fig. 9(b)] as follows:

$$\begin{aligned} &\frac{1}{\|M\|}M|\psi\rangle_{1,2} \\ &\quad = \langle 0|_3 X_1^l \Lambda_{2,3}(Y(-\theta))\Lambda_{1,3}(Y(\theta))X_1^l W_{1,2}|\psi\rangle_{1,2}|0\rangle_3 \\ &\quad \equiv \langle 0|_3 Q|\psi\rangle_{1,2}|0\rangle_3. \end{aligned} \tag{67}$$

From Eqs. (60) and (67) we obtain

$$\langle x|_3\Lambda_{2,3}(Z)\Lambda_{1,3}(Z)|\psi\rangle_{1,2}|+\rangle_3 = \frac{\|M\|}{\sqrt{2}}\langle 0|_3 Q|\psi\rangle_{1,2}|0\rangle_3. \tag{68}$$

[In a mild abuse of the notation, the two types of circuits shown in Figs. 9(a) and 9(b) are both denoted by Q. In the following, the subscript η of Q_η identifies which of these two types of circuits is adopted.]

The type-II projection corresponds to the projection on vertical edge qubits. The projection for each vertical edge qubit is done using

$$\langle x| = x_0\langle 0| + x_1\langle 1| = \frac{e^{\beta J^{\rm v}_{ab}}\langle 0| + e^{-\beta J^{\rm v}_{ab}}\langle 1|}{\sqrt{|e^{\beta J^{\rm v}_{ab}}|^2 + |e^{-\beta J^{\rm v}_{ab}}|^2}}H. \tag{69}$$

The indicator function, angle of the Y rotation, and norm are calculated for each vertical edge qubit $\{a,b\} \in E^{\rm v}$ as follows:

$$l_{ab} = \begin{cases} 0 & \text{if} \quad \left|e^{2\beta J^{\rm v}_{ab}}\right| \geqslant 1, \\ 1 & \text{if} \quad \left|e^{2\beta J^{\rm v}_{ab}}\right| < 1, \end{cases} \tag{70}$$

$$\theta_{ab} = 2\arccos\left(\left|e^{-(-1)^{l_{ab}}2\beta J^{\rm v}_{ab}}\right|\right), \tag{71}$$

$$\|M_{ab}\| = \frac{\sqrt{2}\left|e^{(-1)^{l_{ab}}\beta J^{\mathrm{v}}_{ab}}\right|}{\sqrt{\left|e^{\beta J^{\mathrm{v}}_{ab}}\right|^2 + \left|e^{-\beta J^{\mathrm{v}}_{ab}}\right|^2}}. \tag{72}$$

We have constructed quantum circuits Q_η ($\eta \in V \cup E^{\mathrm{h}} \cup E^{\mathrm{v}}$) that simulate linear operators arising from the MBQC interpretation with the general parameters. Each projection in the overlap mapping equation (9) is replaced with a unitary circuit Q_η, as shown in Fig. 9 (right). Including the initial state and the final readout, this yields

$$Z_{G^{n\times m}} = \Delta_{\mathrm{o}} \langle \alpha | \tilde{G}^{n\times m} \rangle = \Delta \langle 0|^{\otimes |\tilde{V}|} \mathcal{C} |0\rangle^{\otimes |\tilde{V}|}, \tag{73}$$

where the quantum circuit $\mathcal{C}$ is given by

$$\mathcal{C} = \bigotimes_{a\in V_r} A_a \left(\prod_{\eta\in \tilde{V}\setminus V_r}^{\rightarrow} Q_\eta \right) (H^{\otimes n} \otimes I^{\otimes |\tilde{V}-n|}). \tag{74}$$

The product $\vec{\prod}_{\eta\in\tilde{V}\setminus V_r}$ is taken over all qubits on the decorated graph state $|\tilde{G}\rangle$ from left to right except for the vertex qubits at the right boundary. The approximation scale is calculated as

$$\Delta = \Delta_{\mathrm{o}} \prod_{v\in V\setminus V_r} \frac{\|M_v\|}{\sqrt{2}} \prod_{e\in E^{\mathrm{h}}} \frac{\|M_e\|}{\sqrt{2}} \prod_{e\in E^{\mathrm{v}}} \frac{\|M_e\|}{\sqrt{2}}, \tag{75}$$

where the multiplication $\prod_{v\in V\setminus V_r}$ is taken except for the right boundary.

Similar to the unitary case, we can evaluate the matrix element $\langle 0|^{\otimes|\tilde{V}|}\mathcal{C}|0\rangle^{\otimes|\tilde{V}|}$ by using the Hadamard test. Thus, by using a quantum computer, the partition function $Z_{G^{n\times m}}$ with the general coupling strengths and magnetic fields can be approximated with an additive error $\Delta/\mathrm{poly}(n)$. This concludes the extension of the algorithmic domain of the proposed quantum algorithm.

Let us discuss the behavior of the approximation scale. The norm $\|M_\eta\|$ is subject to $1 \leqslant \|M_\eta\| \leqslant \sqrt{2}$ for all $\eta \in V \cup E^{\mathrm{h}} \cup E^{\mathrm{v}}$. If $\|M_\eta\| = 1$ for all $\eta \in V \cup E^{\mathrm{h}} \cup E^{\mathrm{v}}$, the multiplication of $\|M_\eta\|$ is the smallest. In order to achieve this, the coupling strengths and magnetic fields have to satisfy

$$\begin{aligned} \mathrm{Re}(\beta h_a) &= 0, \\ \mathrm{Re}\left(\beta J^{\mathrm{v}}_{ab}\right) &= 0, \\ \mathrm{Im}\left(\beta J^{\mathrm{h}}_{ab}\right) &\in \{(2k+1)\pi/4 | k \in \mathbb{Z}\}, \end{aligned} \tag{76}$$

where $\mathrm{Re}(\cdot)$ and $\mathrm{Im}(\cdot)$ indicate the real and imaginary parts, respectively. These conditions reproduce the algorithmic domain and the approximation scale in the unitary case defined in Problem 1. This is because in the unitary parameter region in Problem 1, the diagonal matrix D becomes an identity, and hence the angle θ of the Y rotation is zero. This decouples the ancilla qubits from the circuits. Then, the unitary gates W and H, as shown in Fig. 9, constitute the unitary circuit constructed in the previous section. When the parameters are changed continuously, the approximation scale Δ is also changed continuously. Thus we expect that an efficient approximation with this approximation scale is also hard for a classical computer around the parameters in Problem 1.

On the other hand, if $\|M_\eta\| = \sqrt{2}$ for all $\eta \in V \cup E^{\mathrm{h}} \cup E^{\mathrm{v}}$, we obtain $\Delta_{\mathrm{o}} = \Delta$, which means that the accuracy of the approximation of the proposed quantum algorithm is equivalent to that of the constant-depth algorithm mentioned in Sec. II. The conditions on the coupling strengths and magnetic fields read

$$\begin{aligned} \mathrm{Re}(\beta h_a) &\to \pm\infty, \\ \mathrm{Re}\left(\beta J^{\mathrm{v}}_{ab}\right) &\to \pm\infty, \\ \mathrm{Re}\left(\beta J^{\mathrm{h}}_{ab}\right) &= 0 \wedge \mathrm{Im}\left(\beta J^{\mathrm{h}}_{ab}\right) \in \{k\pi/2 | k \in \mathbb{Z}\}. \end{aligned} \tag{77}$$

If the parameters are chosen to be finite, then the approximation scale Δ is always smaller than Δ_{o} of the constant-depth algorithm. This indicates that the constructed quantum algorithm gives a better approximation than the constant-depth algorithm in almost all parameter regions.

Let us examine a representative example with $h_a = 1$, $J^{\mathrm{v}}_{ab} = \pm 1$, and $J^{\mathrm{h}}_{ab} = \pm 1$. The partition function is given as a function of the inverse temperature $Z(\beta)$. The signs of the Ising interactions are chosen randomly with a probability of $1/2$. In this case, we can calculate the approximation scale explicitly as follows:

$$\Delta = 2^{nm} e^{(2nm-n-m)\beta} [\cosh(\beta)]^{nm-n} [\cosh(2\beta)]^{n/2}. \tag{78}$$

Accordingly, we can approximate the free energy per site $F(\beta) = \ln Z(\beta)/(nm\beta)$ with an additive error,

$$\epsilon(\beta) \equiv \ln\{1 + \Delta/[\mathrm{poly}(n) Z(\beta)]\}/(nm\beta). \tag{79}$$

Unfortunately, the approximation scale Δ still depends on the size n of the system. Thus an approximation of the free energy per site with an additive error $1/\mathrm{poly}(n)$ cannot be achieved, although this is also the case for other quantum algorithms approximating the Ising partition functions [11,24,28,40].

The accuracy of the proposed algorithm is comparable to that in Ref. [28] (at least in the size of the lattice mentioned), which utilizes an analytical continuation in order to estimate the partition function with real parameters. In the ferromagnetic case without magnetic fields, the scheme in Ref. [28] does a better approximation at lower temperature. This is because the scheme in Ref. [28] intrinsically takes into account the duality between low and high temperatures. On the other hand, the proposed algorithm does not take it into account. For harder instances without any symmetry, we expect that both schemes result in a comparable accuracy.

One advantage of the proposed algorithm is that the approximation scale Δ can be calculated easily. This property would be helpful for comparing other approaches to approximate Ising partition functions. Furthermore, the explicit construction of the unitary circuits that approximate the Ising partition function with the physical parameter region also provides a clue to obtain a classical hardness result, as discussed in the next section.

C. Partial evidence of classical hardness of a multiplicative approximation

We have established a quantum algorithm that approximates the Ising partition functions with the general coupling strengths and magnetic fields. While Problem 1 has been shown to be BQP-complete, it is still unknown whether or not the proposed quantum algorithm performs a nontrivial task in the physical parameter region with real coupling strengths and

magnetic fields. Thus there remains a possibility that a classical algorithm achieves a much better approximation in the physical parameter region. To reduce this possibility, we show partial evidence that an efficient multiplicative approximation cannot be attained by using a classical computer, unless the polynomial hierarchy collapses at the third level, which is highly implausible.

Suppose we have a classical algorithm that approximates the Ising partition functions with an additive error:

$$\left|Z_{G^{n\times m}} - Z^{\mathrm{ap}}_{G^{n\times m}}\right| \leqslant \frac{\epsilon\Delta}{\mathrm{poly}(n)}. \tag{80}$$

Here ϵ indicates the improvement made by the classical algorithm. If $\epsilon\Delta/[Z_{G^{n\times m}}\mathrm{poly}(n)] \leqslant c$ with a constant c, we can approximate the partition function with a multiplicative error as follows:

$$(1-c)Z_{G^{n\times m}} \leqslant Z^{\mathrm{ap}}_{G^{n\times m}} \leqslant (1+c)Z_{G^{n\times m}}. \tag{81}$$

Below we will show partial evidence that there is no classical algorithm that achieves an improvement ϵ such that $c \leqslant 1 - 2^{-1/4}$. To this end, we show the following theorem bridging the physical Ising partition functions and a class of quantum computation, the so-called instantaneous quantum polynomial time computation (IQP) [29,30]:

Definition 1 (IQP). Let n be the number of qubits. A commuting gate is defined by

$$D(\theta_j, S_j) \equiv \exp\left[i\theta_j \prod_{k\in S_j} Z_k\right], \tag{82}$$

where $\theta_j \in [0,2\pi)$ is a real number meaning the rotational angle and $\{S_j\}$ is a set of subsets of $\{1,2,\ldots,n\}$, on which the commuting gates act. We refer to a poly(n) number of commuting gates, including the input state $|+\rangle^{\otimes n}$ and the X-basis measurements, as an IQP circuit. IQP is defined as a sampling problem from the IQP circuit, whose probability distribution is given by

$$P_{\mathrm{IQP}}(\{s_i\}|\{\theta_j\},\{S_j\}) \equiv \left|\bigotimes_{i=1}^{n}\langle +_{s_i}| \prod_j D(\theta_j, S_j)|+\rangle^{\otimes n}\right|^2, \tag{83}$$

where $s_i \in \{0,1\}$ is the measurement outcome and $|+_{s_i}\rangle = Z^{s_i}|+\rangle$.

Theorem 4 (Ising partition functions and IQP). The partition function $Z_{G^{n\times m}}$ of an Ising model on the square lattice $G^{n\times m}$ with real coupling strengths and magnetic fields is equivalent to a probability amplitude of an instance of IQP up to the scale factor

$$\Delta_{\mathrm{IQP}} \equiv \Delta_{\mathrm{o}} 2^{(|V|+|E^{\mathrm{h}}|)/2} \prod_{v\in V}\frac{\|M_v\|}{\sqrt{2}} \prod_{e\in E^{\mathrm{h}}}\frac{\|M_e\|}{\sqrt{2}} \prod_{e\in E^{\mathrm{v}}}\frac{\|M_e\|}{\sqrt{2}}. \tag{84}$$

Proof. Here we consider another quantum circuit

$$\mathcal{C}' = \prod_{\eta\in\tilde{V}}^{\rightarrow} Q_\eta, \tag{85}$$

acting on $n + |\tilde{V}|$ qubits, where the initial and final states are $|+\rangle^{\otimes n}|0\rangle^{\otimes|\tilde{V}|}$ and $\langle+|^{\otimes n}\langle 0|^{\otimes|\tilde{V}|}$, respectively. This quantum circuit also satisfies

$$Z_{G^{n\times m}} = \Delta'\langle+|^{\otimes n}\langle 0|^{\otimes|\tilde{V}|}\mathcal{C}'|+\rangle^{\otimes n}|0\rangle^{\otimes|\tilde{V}|}, \tag{86}$$

with the approximation scale

$$\Delta' = \Delta_{\mathrm{o}} 2^{n/2} \prod_{v\in V}\frac{\|M_v\|}{\sqrt{2}} \prod_{e\in E^{\mathrm{h}}}\frac{\|M_e\|}{\sqrt{2}} \prod_{e\in E^{\mathrm{v}}}\frac{\|M_e\|}{\sqrt{2}}. \tag{87}$$

(In contrast to the previous case, the final projection is also simulated in $\mathcal{C}'$, and hence the approximation scale Δ' is slightly different from Δ.)

The quantum circuit $\mathcal{C}'$ consists of single-qubit gates $\{X^l, H\}$, and two-qubit gates $\Lambda(Y(\theta))$ since W becomes an identity gate in the physical parameter region. By using a single-qubit Clifford gate $R = (X+Z+Y+iI)/2$, the Y rotation can be transformed into a Z rotation $Z(\theta) = e^{-i\theta Z/2}$ [see Fig. 10(a)]. Then the initial and final states of the ancilla qubit are transformed into $|+\rangle$ and $\langle+|$, respectively. Thus we obtain

$$Z_{G^{n\times m}} = \Delta'\langle+|^{\otimes n+|\tilde{V}|}\mathcal{D}|+\rangle^{\otimes n+|\tilde{V}|}, \tag{88}$$

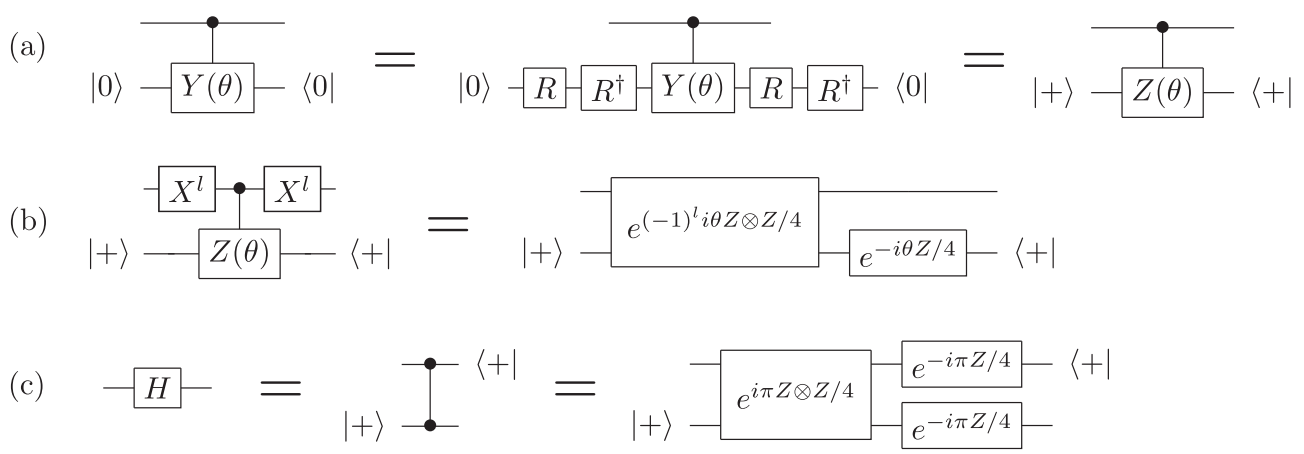

FIG. 10. (a) A circuit equivalence between controlled-Y and controlled-Z rotation gates. (b) Transforming a controlled-Z gate to rotational gates with respect to the operators Z and $Z\otimes Z$, where X^l is taken in the rotational angle. (c) A measurement-based implementation of the Hadamard gate.

where $\mathcal{D}$ is obtained from $\mathcal{C}'$ by replacing all controlled-Y rotations $\Lambda(Y(\theta))$ with controlled-Z rotations $\Lambda(Z(\theta))$.

The controlled-Z rotation is decomposed into single- and two-qubit Z rotations:

$$\Lambda_{a,b}(Z(\theta)) = e^{i\theta Z_a Z_b/4} e^{-i\theta Z_b/4}. \tag{89}$$

The two X_a^l gates before and after $\Lambda_{a,b}(Z(\theta))$ are absorbed into the rotational angles [see Fig. 10(b)],

$$X_a^l \Lambda_{a,b}(Z(\theta)) X_a^l = e^{(-1)^l i\theta Z_a Z_b/4} e^{-i\theta Z_b/4}. \tag{90}$$

The Hadamard gate can be implemented using an ancilla qubit $|+\rangle$, the two-qubit gate $\Lambda(Z)$, and the projection $\langle +|$ in a teleportation-based way [see Fig. 10(c)]. The $\Lambda(Z)$ gate can also be represented as single- and two-qubit Z rotations:

$$\Lambda_{a,a'}(Z) = e^{-i\pi/4} e^{i\pi Z_a Z_{a'}/4} e^{-i\pi Z_a/4} e^{-i\pi Z_{a'}/4}, \tag{91}$$

where the subscripts a and a' denote the labels of the input and output qubits of the gate teleportation.

Accordingly, the circuit $\mathcal{D}$ can be reformulated as a commuting circuit $\mathcal{D}'$ acting on the qubits on graph G' as shown in Fig. 11:

$$\begin{aligned}&\langle +|^{\otimes n+|\tilde{V}|} \mathcal{D} |+\rangle^{\otimes n+|\tilde{V}|} \\ &\quad = 2^{(|V|+|E^{\mathrm{h}}|-n)/2} \langle +|^{\otimes |\tilde{V}|+|V|+|E^{\mathrm{h}}|} \mathcal{D}' |+\rangle^{\otimes |\tilde{V}|+|V|+|E^{\mathrm{h}}|},\end{aligned} \tag{92}$$

where the final Hadamard gates are taken by the final state $\langle +|$ without teleportation and the number of qubits is equal to that of vertices $|V'| = |\tilde{V}| + |V| + |E^{\mathrm{h}}|$ of G'. The commuting circuit $\mathcal{D}'$ consists of only single- and two-qubit Z rotations with appropriately chosen angles $\{\tilde{\theta}_{ab}, \tilde{\theta}_a\}$ (see also Fig. 12):

$$\mathcal{D}' = \prod_{\{a,b\}\in E'} e^{i\tilde{\theta}_{ab} Z_a Z_b} \prod_{a\in V'} e^{i\tilde{\theta}_a Z_a}, \tag{93}$$

where the multiplication is taken over the set of edges E' and the set of vertices V' of graph G'. The matrix element on the rhs of Eq. (92) is regarded as a probability amplitude of an instance of the IQP circuit. Specifically, the corresponding IQP circuit consists of single-qubit and nearest-neighbor two-qubit commuting gates acting on a 2D graph G'. Then, we obtain the correspondence between the Ising partition function and the probability amplitude of the IQP circuit,

$$Z_{G^{n\times m}} = \Delta' 2^{(|V|+|E^{\mathrm{h}}|-n)/2} \langle +|^{\otimes |V'|} \mathcal{D}' |+\rangle^{\otimes |V'|}. \tag{94}$$

■

Suppose the partition function $Z_{G^{n\times m}}$ can be approximated with a multiplicative error $2^{1/4}$, that is,

$$2^{-1/4} Z_{G^{n\times m}} \leqslant Z^{\mathrm{ap}}_{G^{n\times m}} \leqslant 2^{1/4} Z_{G^{n\times m}}. \tag{95}$$

Due to Theorem 4, this means that we can approximate the probability of the output of the corresponding IQP circuit with a multiplicative error $\sqrt{2}$. On the other hand, as shown in Refs. [29,30], even a weak simulation of a large class of IQP circuits with the multiplicative error $\sqrt{2}$ is hard for a classical computer unless the polynomial hierarchy collapses at the third level, which is highly implausible. A strong simulation, the calculation of a probability distribution, is much harder than a weak simulation, which samples the outcomes according to the distribution [41]. Thus we reasonably conjecture that there is no efficient classical algorithm that approximates the Ising partition functions in the physical parameter region with a multiplicative error $2^{1/4}$. (By considering a polynomial number of replicas of $Z_{G^{n\times m}}$, the multiplicative error can be improved to be $2^{1/\mathrm{poly}(n)}$, although the following final result does not change.) If this conjecture is true, the classical improvement of the approximation scale ϵ is limited to $\epsilon \geqslant (1 - 2^{-1/4})\mathrm{poly}(n) Z_{G^{n\times m}}/\Delta$. Since we are interested only in the exponential behavior, a possible improvement of the approximation scale by a classical algorithm is $\epsilon \sim Z_{G^{n\times m}}/\Delta$.

For the ferromagnetic Ising models with a constant magnetic field on arbitrary graphs, a fully polynomial randomized approximation scheme (FPRAS) has been shown to exist [9]. However, under the random magnetic fields, approximation of ferromagnetic Ising partition functions belong, under an approximation-preserving reduction, to the class #BIS, which is defined as a counting problem of the number of independent sets of a bipartite graph [42]. The class #BIS is known to lie in between FPRAS and #SAT under an approximation-preserving reduction. Here #SAT indicates a counting problem of the number of satisfying configurations and does not have an efficient (polynomial) multiplicative approximation unless NP = PR [7]. Moreover, it has been shown that a multiplicative approximation of antiferromagnetic Ising partition functions on d-regular graphs ($d \geqslant 3$) are NP-hard [43]. While an efficient approximation of Ising partition functions on the square lattices would still not be excluded, these facts and the above partial evidence support the possibility that the proposed quantum algorithm of an additive approximation performs a nontrivial task even in the physical parameter region.

There is also another interesting corollary of Theorem 4.

Corollary 1 (real-imaginary correspondence). An arbitrary Ising partition function $Z_{G^{n\times m}}$ on a square lattice $G^{n\times m}$ with real parameters can be mapped into an Ising partition function $Z_{G'}$ on a lattice G', shown in Fig. 11(b), with imaginary parameters with a scale factor $\Delta' 2^{-5nm+2n+m}$:

$$Z_{G^{n\times m}} = \Delta' 2^{-5nm+2n+m} Z_{G'}. \tag{96}$$

Proof. In Ref. [29], a correspondence between IQP and Ising partition functions with imaginary parameters has been established. It indicates that the matrix element on the rhs of Eq. (94) is equivalent to an Ising partition function $Z_{G'}$ on a lattice G' with imaginary parameters with a scale factor $2^{|V'|}$:

$$Z_{G'} = 2^{|V'|} \langle +|^{\otimes |V'|} \mathcal{D}' |+\rangle^{\otimes |V'|}. \tag{97}$$

Combining Eq. (97) with Theorem 4, we obtain

$$Z_{G^{n\times m}} = \Delta' 2^{(|V|+|E^{\mathrm{h}}|-n)/2} 2^{-|V'|} Z_{G'} = \Delta' 2^{-5nm+2n+m} Z_{G'}. \tag{98}$$

■

There has been a transformation, such as a duality transformation [44], that maps an Ising partition function with a real coupling strength into an imaginary one for a restricted case. However, Corollary 1 can be applied for Ising models with arbitrary real coupling strengths and magnetic fields. Since imaginary and real Ising partition functions have been well studied in quantum and classical information, respectively, the real-imaginary correspondence would be useful to bridge these two fields.

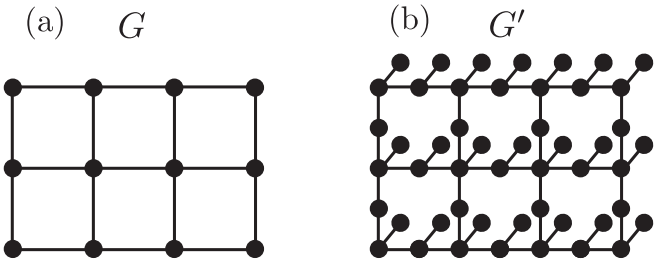

FIG. 11. (a) Graph G, on which the Ising model with real parameters is defined. (b) Graph G', on which the commuting circuits for IQP are defined. The Ising model with imaginary parameters is also defined on graph G'.

V. CONCLUSIONS AND DISCUSSION

We have constructed a quantum algorithm for an additive approximation of the partition functions of Ising models on square lattices. Specifically, we have argued both BQP-completeness [23,31] and the extension toward the physical parameter region [24] within the same model. This allows us to calculate the approximation scale explicitly and to investigate the behavior of the approximation scale penetrating from the unitary case (Problem 1), which includes the BQP-complete problem, to the physical parameter region, which is of central interest in statistical physics and computer science. We have shown that the MBQC interpretation always provides a better approximation than the constant-depth straightforward quantum algorithm as long as the coupling strengths and magnetic fields are finite.

The overlap mapping and the MBQC interpretation are quite useful for translating the partition functions into quantum circuits and calculating the resultant approximation scale. While we have only considered square lattices, this method could also be generalized to the Ising models on general lattice structures. In such a case, the MBQC interpretation is made on general graph states. In this context, flow theory and its generalization, gflow [45,46], would provide an efficient scheme to construct the corresponding quantum circuits.

Compared to the recent related work [28] based on an analytical continuation, the proposed construction with linear operator simulations provides a comparable approximation error for the random-bond Ising models with magnetic fields (at least with the size mentioned in Ref. [28]). One advantage of the proposed algorithm in the physical parameter region is that the approximation scale can be easily obtained, which allows us to compare the performance with other approaches.

We have also provided partial evidence that there is no efficient classical algorithm for a multiplicative approximation of the Ising partition functions in the physical parameter

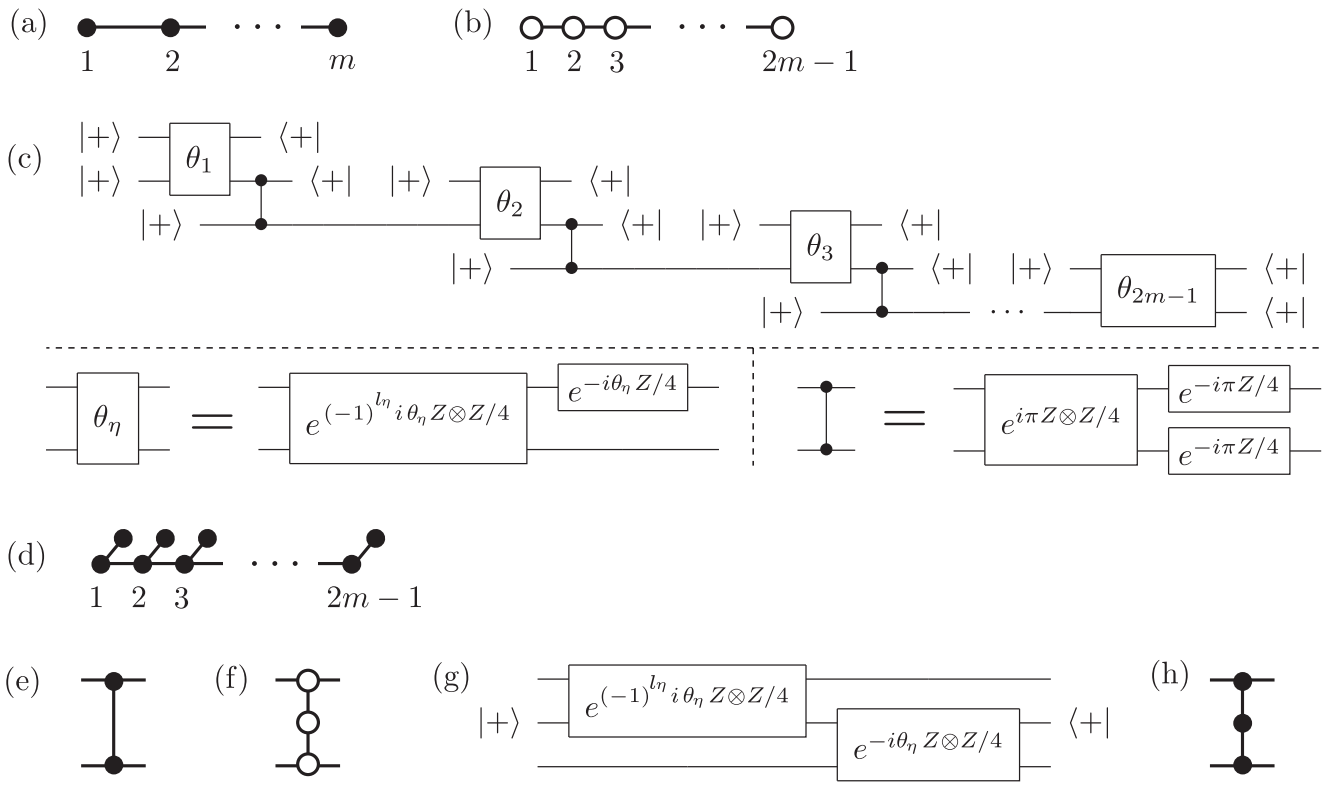

FIG. 12. The correspondence between the Ising models with real and imaginary parameters on a square lattice G and another lattice G', respectively. (a)–(d) A 1D lattice with magnetic fields and horizontal couplings (i.e., $n = 1$). (a) A 1D lattice G. (b) The corresponding decorated graph state $|\tilde{G}\rangle$. (c) A quantum circuit $\mathcal{D}'$, which is decomposed into single- and two-qubit Z-rotation gates, as shown in Fig. 10. (d) Graph G', on which the Ising model with imaginary parameters is defined. (e) A vertical coupling for the case of a square lattice G. (f) The corresponding decorated graph state $|\tilde{G}\rangle$. (g) The corresponding unitary gate in $\mathcal{D}'$. (h) The corresponding part of graph G', on which the Ising model with imaginary parameters is defined. By combining (a)–(d) and (e)–(h) we can obtain Theorem 4.

region. This has been shown by relating the quantum circuit that corresponds to the Ising partition functions to an IQP circuit. On the other hand, in the unitary case, the problem (Problem 1) that can be solved by the proposed quantum algorithm is BQP-complete. These facts strongly support the observation that the proposed quantum algorithm performs a nontrivial task even in the physical parameter regime with real coupling strengths and magnetic fields.

Unfortunately, it is still not known whether the proposed quantum algorithm performs a nontrivial task inside the physical parameter region. However, the problems that we have to tackle are now made clear. First, we have to rigorously prove that classical simulation (strong simulation with a multiplicative error) of the related IQP circuits is hard. This could be solved by clarifying whether or not the IQP circuits become universal for quantum computation with the help of postselection [29,30]. Second, we have to find a quantum algorithm or instances of the parameters that attain a multiplicative approximation. Otherwise, we have to show that an additive approximation with the approximation scale Δ is still hard for a classical computer. In doing so, the quantum circuits we have constructed would provide us with a clue. If these problems were solved, we could have another nontrivial quantum algorithm that solves quite important problems in statistical mechanics and computer science.

ACKNOWLEDGMENTS

K.F. is supported by JSPS Grant-in-Aid for Research Activity Start-up No. 25887034. This work was supported by JSPS Grant-in-Aid for Scientific Research(A) No. 25247068.

[1] T. D. Lee and C. N. Yang, Phys. Rev. **87**, 410 (1952).
[2] J. J. Hopfield, Proc. Natl. Acad. Sci. USA **79**, 2554 (1982).
[3] S. N. Durlauf, Proc. Natl. Acad. Sci. USA **96**, 10582 (1999).
[4] P. W. Kasteleyn, Physica (Amsterdam) **27**, 1209 (1961).
[5] M. E. Fisher, J. Math. Phys. **7**, 1776 (1966).
[6] F. Barahona, J. Phys. A: Math. Gen. **15**, 3241 (1982).
[7] D. Zuckerman, SIAM J. Comput. **25**, 1293 (1996).
[8] RP (randomized polynomial time computation) is a class of problems solvable by a probabilistic Turing machine in the following sense: if the correct answer is no, it always returns no. If the correct answer is yes, it returns yes with a probability of at least 1/2. RP trivially includes P (polynomial time computation); hence RP = NP also implies P = NP and hence is believed to be highly implausible.
[9] M. Jerrum and A. Sinclair, SIAM J. Comput. **22**, 1087 (1993).
[10] L. A. Goldberg and M. Jerrum, Inf. Comput. **206**, 908 (2008).
[11] C. P. Master, F. Yamaguchi, and Y. Yamamoto, Phys. Rev. A **67**, 032311 (2003).
[12] D. A. Lidar and O. Biham, Phys. Rev. E **56**, 3661 (1997).
[13] R. Raussendorf and H. J. Briegel, Phys. Rev. Lett. **86**, 5188 (2001); R. Raussendorf, D. E. Browne, and H. J. Briegel, Phys. Rev. A **68**, 022312 (2003).
[14] S. Bravyi and R. Raussendorf, Phys. Rev. A **76**, 022304 (2007).
[15] M. Van den Nest, W. Dür, and H. J. Briegel, Phys. Rev. Lett. **98**, 117207 (2007).
[16] K. Fujii, Interdiscip. Inf. Sci. **19**, 1 (2013).
[17] M. Van den Nest, W. Dür, and H. J. Briegel, Phys. Rev. Lett. **100**, 110501 (2008).
[18] V. Karimipour and M. H. Zarei, Phys. Rev. A **86**, 052303 (2012).
[19] G. De las Cuevas, W. Dür, H. J. Briegel, and M. A. Martin-Delgado, Phys. Rev. Lett. **102**, 230502 (2009).
[20] G. De las Cuevas, W. Dür, H. J. Briegel, and M. A. Martin-Delgado, New J. Phys. **12**, 043014 (2010).
[21] Ying Xu, G. De las Cuevas, W. Dür, H. J. Briegel, and M. A. Martin-Delgado, J. Stat. Mech.: Theory Exp. (2011) P02013.
[22] M. Van den Nest and W. Dür, Phys. Rev. A **89**, 012334 (2014).
[23] G. De las Cuevas, W. Dür, M. Van den Nest, and M. A. Martin-Delgado, New J. Phys. **13**, 093021 (2011).
[24] I. Arad and Z. Landau, SIAM J. Comput. **39**, 3089 (2010).
[25] D. Aharonov, V. Jones, and Z. Landau, in *Proceedings of the 38th Annual ACM Symposium on Theory of Computing (STOC 2006)* (ACM Press, New York, 2006), pp. 427–436.
[26] D. Aharonov, I. Arad, and Z. Landau, arXiv:quant-ph/0702008.
[27] D. Aharonov and I. Arad, New J. Phys. **13**, 035019 (2011).
[28] S. Iblisdir, M. Cirio, O. Boada, and G. K. Brennen, Ann. Phys. (NY) **340**, 205 (2014).
[29] K. Fujii and T. Morimae, arXiv:1311.2128.
[30] M. J. Bremner, R. Jozsa, and D. J. Shepherd, Proc. R. Soc. A **467**, 459 (2010).
[31] M. Van den Nest, W. Dür, R. Raussendorf, and H. J. Briegel, Phys. Rev. A **80**, 052334 (2009).
[32] M. Hein, W. Dür, J. Eisert, R. Raussendorf, M. V. den Nest, and H.-J. Briegel, in *Proceedings of the International School of Physics, "Enrico Fermi" on Quantum Computers, Algorithms and Chaos* (Varenna, Italy, 2005), Vol. 162.
[33] M. Hein, J. Eisert, and H. J. Briegel, Phys. Rev. A **69**, 062311 (2004).
[34] E. Bernstein and U. Vazirani, in *Proceedings of the 25th Annual ACM Symposium on the Theory of Computing (STOC), 1993* (Association for Computing Machinery, New York, 1996), p. 11; SIAM J. Comput. **26**, 1411 (1997).
[35] M. A. Neilsen and I. L. Chuang, *Quantum Computation and Quantum Information* (Cambridge University Press, Cambridge, 2000).
[36] R. Raussendorf, Phys. Rev. A **72**, 022301 (2005).
[37] A. Broadbent, J. Fitzsimons, and E. Kashefi, in *Proceedings of the 50th Annual IEEE Symposium on Foundations of Computer Science (FOCS 2009)* (IEEE Press, Piscataway, NJ, 2009), pp. 517–526.
[38] T. Morimae and K. Fujii, Phys. Rev. A **87**, 050301(R) (2013).
[39] D. Schlingemann, Quantum Inf. Comput. **4**, 287 (2004).
[40] M. H. Yung, D. Nagaj, J. D. Whitfield, and A. Aspuru-Guzik, Phys. Rev. A **82**, 060302 (2010).
[41] Actually, if a quantum computational class A satisfies post-A = post-BQP, then a strong simulation of A is #P-hard [29].
[42] L. A. Goldberg and M. Jerrum, J. Combinatorics, Probab. Comput. **16**, 43 (2006).
[43] A. Sly and N. Sun, in *Proceedings of the 50th Annual IEEE Symposium on Foundations of Computer Science (FOCS 2012)* (IEEE Press, Piscataway, NJ, 2012), pp. 361–369.
[44] H. A. Kramers and G. H. Wannier, Phys. Rev. **60**, 252 (1941).
[45] V. Danos and E. Kashefi, Phys. Rev. A **74**, 052310 (2006).
[46] D. E. Browne, E. Kashefi, M. Mhalla, and S. Perdrix, New J. Phys. **9**, 250 (2007).